Article

A discrete neuronal population coordinates brain-wide developmental activity

https://doi.org/10.1038/s41586-022-04406-9

Received: 27 February 2021

Accepted: 5 January 2022

Published online: 09 February 2022

Check for updates

Bryce T. Bajar[1], Nguyen T. Phi[2], Jesse Isaacman-Beck[3], Jun Reichl[4], Harpreet Randhawa[4] & Orkun Akin[4]✉

In vertebrates, stimulus-independent activity accompanies neural circuit maturation throughout the developing brain[1,2]. The recent discovery of similar activity in the developing *Drosophila* central nervous system suggests that developmental activity is fundamental to the assembly of complex brains[3]. How such activity is coordinated across disparate brain regions to influence synaptic development at the level of defined cell types is not well understood. Here we show that neurons expressing the cation channel transient receptor potential gamma (Trpγ) relay and pattern developmental activity throughout the *Drosophila* brain. In *trpγ* mutants, activity is attenuated globally, and both patterns of activity and synapse structure are altered in a cell-type-specific manner. Less than 2% of the neurons in the brain express Trpγ. These neurons arborize throughout the brain, and silencing or activating them leads to loss or gain of brain-wide activity. Together, these results indicate that this small population of neurons coordinates brain-wide developmental activity. We propose that stereotyped patterns of developmental activity are driven by a discrete, genetically specified network to instruct neural circuit assembly at the level of individual cells and synapses. This work establishes the fly brain as an experimentally tractable system for studying how activity contributes to synapse and circuit formation.

Understanding how specific synaptic connections are established during development is a fundamental challenge in neurobiology. During circuit formation, stimulus-independent neural activity is known to contribute to synapse development. Such developmental activity has been observed throughout the developing central nervous system[1,2] (CNS). For example, retinal waves initiate in the eye, propagate to higher-order visual centres[4–6] and contribute to eye-specific segregation and refinement of retinotopy[7–9].

The integration of different visual centres with activity raises the possibility of broader coordination of circuit assembly across other interconnected regions of the brain through developmental activity. The size and complexity of vertebrate models pose challenges to exploring this question of scale. Notably, the same challenges have also checked progress at the cellular level, where our understanding of the role of activity on cell-type-specific synaptic development remains limited.

Activity has been shown to accompany the development of the adult nervous system in *Drosophila melanogaster*[3], challenging the view that neural circuit assembly in invertebrates occurs independently of activity[10,11]. The adult CNS of the fly is built during the 100 h of pupal development; synapse formation takes place in the latter half of this period[12,13]. Patterned, stimulus-independent neuronal activity (PSINA) coincides with synaptogenesis, starting at approximately 50 h after puparium formation[3] (hAPF). The entire CNS participates in PSINA, which is characterized by periodic active and silent phases coordinated throughout the brain (Fig. 1a). Each active phase consists of multiple bouts of neural activity, termed sweeps. PSINA evolves from a periodic stage with regular active phases to a more irregular turbulent stage at around 70 hAPF. The brain-wide coordination of PSINA suggests a global mechanism that stands in contrast to existing models of local activity initiation[1].

PSINA has previously been characterized in the visual system[3], which contains three neuropils: the lamina, medulla and lobula complex. The optic neuropils are organized by columns, which are repetitive, retinotopic relays that map the input from the compound eye, and by distinct layers where different visual circuits make connections. The synaptic connectivity of the more than 100 cell types populating these neuropils has been determined by dense electron microscopic reconstruction[14]. Visual system neurons participate in PSINA with individualized activity patterns that reflect adult connectivity, suggesting that PSINA may have a role in synapse formation in a cell-type-specific manner.

Here we report that a population of neurons that express Trpγ is necessary for the patterning and propagation of PSINA throughout the brain. Disruption of PSINA in *trpγ* mutants leads to altered synapse counts in visual processing neurons, indicating that activity contributes to synaptogenesis in a cell-type-specific manner. These results provide insight into the coordination of developmental activity across the CNS and establish a role for stimulus-independent activity in synapse development.

[1]Department of Biological Chemistry, Medical Scientist Training Program, David Geffen School of Medicine at UCLA, University of California, Los Angeles, Los Angeles, CA, USA. [2]Molecular, Cellular, and Integrative Physiology Interdepartmental Graduate Program, University of California, Los Angeles, Los Angeles, CA, USA. [3]Department of Neurobiology, Stanford University School of Medicine, Stanford University, Stanford, CA, USA. [4]Department of Neurobiology, David Geffen School of Medicine at UCLA, University of California, Los Angeles, Los Angeles, CA, USA. ✉e-mail: akin.orkun@gmail.com

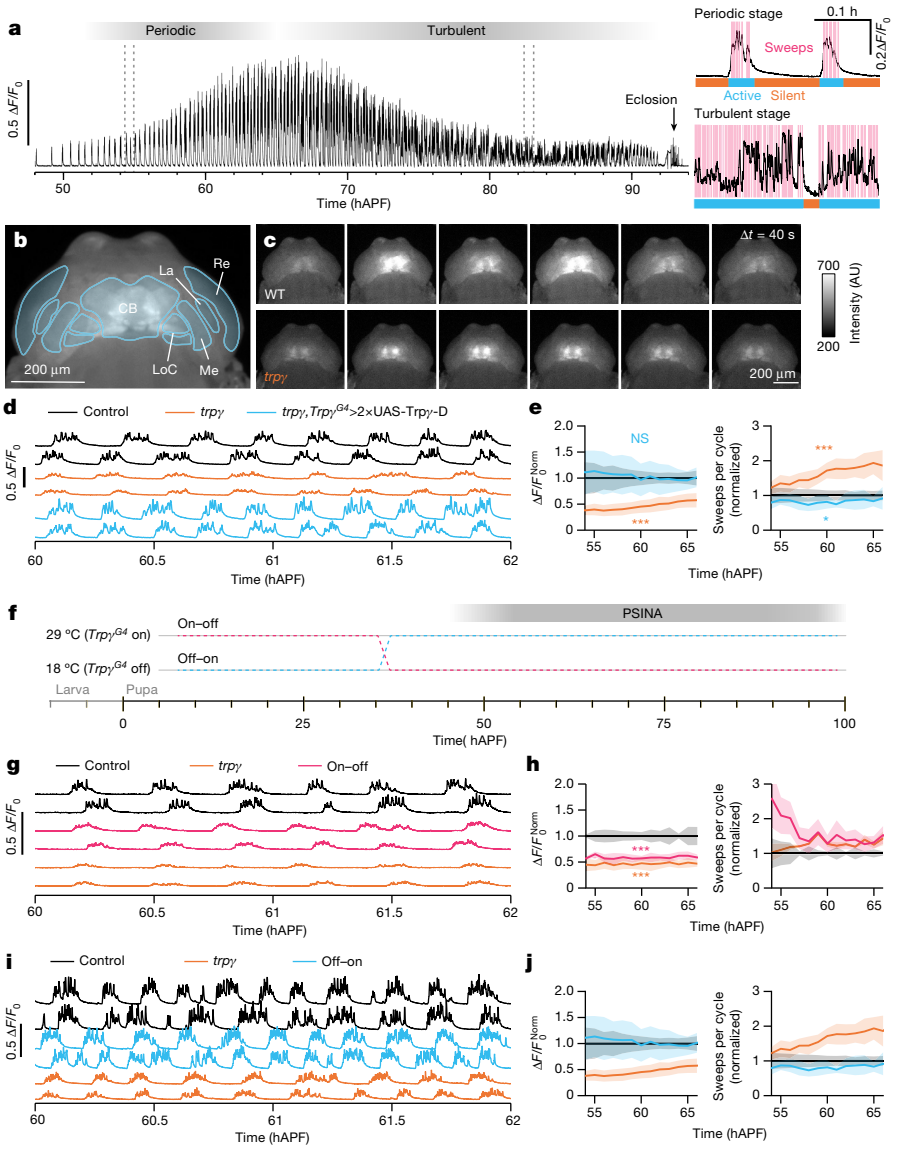

Fig. 1 | *Trpγ* is necessary for wild-type PSINA. a, Representative trace of PSINA, recorded with wide-field fluorescence imaging from a pupa expressing pan-neuronal GCaMP6s. This fly eclosed at approximately 93 hAPF. Dotted lines mark limits of inset traces (right) from periodic (top) and turbulent (bottom) stages. Highlights (magenta) mark individual sweeps; bars mark active (cyan) and silent (orange) phases. **b**, Average intensity projection (AIP) from wide-field fluorescence series of a pupa expressing pan-neuronal GCaMP6s. CB, central brain; La, lamina; Re, retina; LoC, lobula complex; Me, medulla. Scale bar, 200 µm. **c**, Images spanning one active phase at 60 hAPF in control (top) and *trpγ*-mutant pupae (bottom). Frames are approximately 40 s apart. Scale bar, 200 µm. **d**, **e**, PSINA traces (**d**) and active phase average amplitude ($\Delta F/F_0^{Norm}$, left) and sweeps per cycle (right) (**e**) binned by hour and normalized to control in control (black, $n = 19$ flies), *trpγ* (orange, $n = 31$ flies) and *trpγ*, $Trpγ^{G4}$ > 2xUAS-Trpγ-D (cyan, $n = 4$ flies) flies. Shaded areas in **e** indicate s.d. **f**, Expression control of UAS-Trpγ-D with TARGET (GAL80ts); temperature shift at 36 hAPF. **g**, **h**, PSINA traces (**g**) and active phase average amplitude (left) and sweeps per cycle (right) (**h**) in control (black, $n = 8$ flies), *trpγ* (orange, 8 flies) and 'on–off' pupae (magenta, $n = 5$ flies) binned by hour and normalized to control. **i**, **j**, PSINA traces (**i**) and active phase average amplitude (left) and sweeps per cycle (right) (**j**) in control (black, $n = 3$ flies), *trpγ* (orange, $n = 3$ flies) and 'off–on' pupae (cyan, $n = 3$ flies) binned by hour and normalized to control. $^*P < 0.05$; $^{**}P < 0.01$; $^{***}P < 0.001$ by Welch's *t*-test following Shapiro–Wilk test, tested against control at 60 hAPF. AU, arbitrary units; NS, not significant ($P > 0.05$). Detailed genotypes in this and other figures listed in Supplementary Table 1.

Trpγ is necessary and sufficient for PSINA

Using a targeted screen of 7 transient receptor potential (TRP) channels with viable null mutants (7 out of 13 TRPs in *Drosophila*[15]), we found that PSINA is attenuated in mutants of *trpγ*. In mutant pupae expressing GCaMP6s[16] in pan-neuronal fashion (Fig. 1b, c, Extended Data Fig. 1a), PSINA amplitude is reduced during the periodic stage (55–65 hAPF, 45 ± 12% at 60 hAPF) and the turbulent stage (70 hAPF through eclosion, 73 ± 20% at 75 hAPF) relative to heterozygous controls (Fig 1b–e, Extended Data Fig. 1a, b, Supplementary Video 1). By contrast, the number of sweeps per active phase increases by up to twofold (Fig 1e, Extended Data Fig. 1a, b). The duration or frequency of cycles does not change significantly (Extended Data Fig. 1c). Genetic complementation analysis carried out with a *Trpγ* gene trap[17] ($Trpγ^{G4}$), a Drop-In allele[18] ($Trpγ^{DropIn\text{-}TG4}$), and two deficiencies confirmed that the described PSINA phenotype is monogenic (Extended Data Fig. 1d, e). The PSINA phenotype does not affect eclosion: *trpγ* mutants eclose at the same rate as wild type (>98%), and their lifespan is largely unaffected (50% survival at about 70 days for wild-type and *trpγ*-null females, and about 60 and 50 days for wild-type and *trpγ*-null males,

respectively). Trpγ has been reported to interact with Trp and TrpL[19]. *Trp* and *trpL* mutants did not have altered PSINA, and *trp trpγ* or *trpL trpγ* double mutants did not further attenuate PSINA (Extended Data Fig. 1f, g). These results indicate that *Trpγ* is necessary for wild-type PSINA.

The *Trpγ* gene produces three isoforms: Trpγ-A, Trpγ-B[19] and Trpγ-D[20] (Extended Data Fig. 2a). When expressed under $Trp\gamma^{G4}$, the common coding sequence for Trpγ-A and Trpγ-B (that is, Trpγ-AB) rescues fine motor defects of otherwise viable and fertile *trpγ* mutant flies in the adult[17]. More recently, Trpγ-D was identified in a high-throughput study of development-specific promoter use[20]. Compared with Trpγ-AB, Trpγ-D has an additional 60-amino-acid N-terminal leader sequence; however, its function remains unknown. $Trp\gamma^{G4}$-driven expression of Trpγ-D results in complete rescue of PSINA in a dose-dependent manner (Fig. 1d, Extended Data Fig. 2b, c). Driving Trpγ-D with the independently generated $Trp\gamma^{DropIn\text{-}TG4}$ allele produces similar results (Extended Data Fig. 2b, c), confirming the efficacy of these transgenic reagents in capturing the *Trpγ* expression domain (that is, Trpγ+ cells). In contrast to Trpγ-D, Trpγ-AB does not rescue sweep dynamics, and combined expression of Trpγ-AB and Trpγ-D rescues amplitude but produces an altered rhythm (Extended Data Fig. 2b, c). These results indicate that the Trpγ-D isoform, expressed in Trpγ+ cells, is sufficient for wild-type PSINA.

To establish when Trpγ-D is required, we used the TARGET system[21] to control the timing of Trpγ-D expression (Fig. 1f, Extended Data Fig. 2d–h). Expression of Trpγ-D throughout development up to the onset of PSINA does not rescue the mutant phenotype (Fig. 1g, h). By contrast, the reciprocal expression control scheme leads to rescue similar to constitutive Trpγ-D expression (Fig. 1i, j).

We conclude that Trpγ-D expression in Trpγ+ cells during the second half of pupal development is necessary and sufficient for wild-type PSINA.

PSINA dynamics are *Trpγ*-dependent

To characterize the *trpγ* phenotype at the level of cell types, we followed PSINA in the visual system of developing pupae using two-photon microscopy[22]. We focused on 10 cell types (Fig. 2a), representing major classes of visual processing neurons, including lamina monopolar neurons (L1, L3 and L5), medulla intrinsic neurons (Mi1 and Mi4), transmedullary neurons (Tm3, Tm4 and Tm9), and T4/5 neurons. At the population level, cells of a type begin the periodic stage of PSINA (55–65 hAPF) with fewer cycles per hour in the mutant; the cycle frequency gradually becomes similar to the wild type (Fig. 2b). Although the active phase duration of these cycles are similar across wild-type and mutant flies, the sweep count per cycle is higher in the *trpγ* background (Fig. 2b), consistent with pan-neuronal trends (Extended Data Fig. 1a).

At the cellular level, visual system neurons display cell-type-specific PSINA dynamics ranging from synchronous bursts of activity to wave-like patterns[3]. To compare activity across cell types and genotypes, two scalar metrics were previously developed: 'coordination' is the average fraction of cells that participate in each sweep; and 'coherence' is the largest fraction of cells that peak within the same time point, averaged over all sweeps[3]. In the *trpγ* background, all cell types have lower coordination and nearly all cell types have higher coherence (Fig. 2c–h, Supplementary Video 2). Lower coordination indicates that fewer cells of a type participate in each sweep, suggesting that the pan-neuronal loss of PSINA amplitude in mutant flies is owing to reduced overall neuronal participation (Fig. 1d, e). The opposite trend in coherence reports a shift away from wave-like activity propagation in favour of more synchronous populations. L5 is the lone exception to this trend in coherence. Together, these results indicate that *Trpγ* is necessary for wild-type, cell-type-specific PSINA dynamics in visual processing neurons.

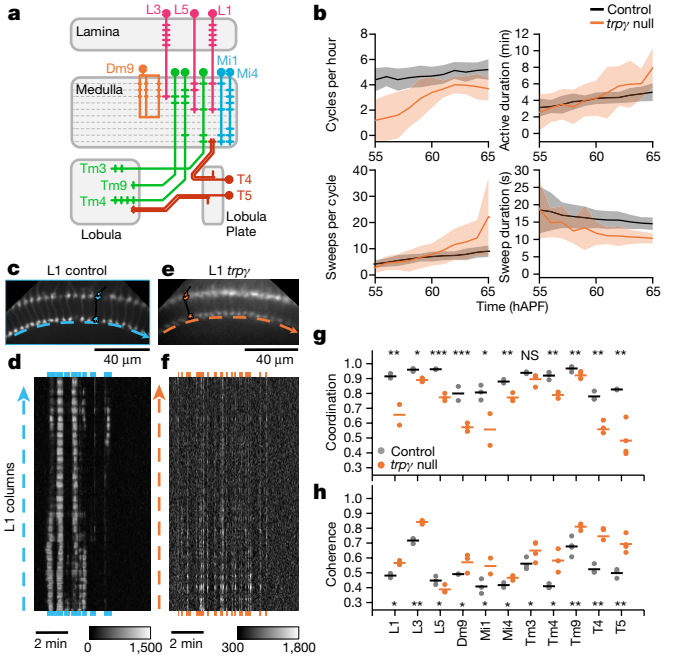

Fig. 2 | Activity patterns in visual processing neurons are altered in *trpγ* mutants. a, Schematic of visual system cell types studied. **b**, Average metrics pooled from two-photon microscopy imaging of all cell types in control (black, $n = 31$ flies) and *trpγ* (orange, $n = 33$ flies) pupae. Shaded areas indicate s.d. **c**, **e**, AIP of L1 medulla projections in control (**c**) and *trpγ* (**e**) pupae. Cartoons illustrate single L1s in each array. Dashed arrows sit below thin profiles used to generate the kymographs in **d**, **f**; arrow direction matches layout of kymographs. **d**, **f**, Kymographs of net fluorescence from profiles in **c**, **e**, showing one active phase (approximately 60 hAPF) with sweeps highlighted in blue (**d**) or orange (**f**). **g**, **h**, Coordination (**g**) and coherence (**h**) values over 55–65 hAPF calculated for different cell types in control (black) or *trpγ* (orange) pupae. Round markers are values from individual time series, bars are averages for each cell type. $n = 2$–3 time series for each cell type. $^*P < 0.05$; $^{**}P < 0.01$; $^{***}P < 0.001$ by Welch's *t*-test following Shapiro–Wilk test.

Synaptogenesis depends on PSINA

To assess whether loss of *Trpγ* affects synapse formation, we used the synaptic tagging with recombination (STaR) technique, which enables cell-specific labelling of the active zone structural protein Bruchpilot (Brp)[12]. As the labelled Brp is expressed at physiological levels with STaR, wild-type synapse counts track closely with those reported in electron microscopy reconstructions, particularly for cells with sparser active zones such as R8 and L4[14,23] (Extended Data Fig. 3a). There are other neurons, such as Mi1, for which STaR under-reports the actual synapse count owing to resolution constraints. Although we refer to STaR-derived data as synapse count, reported changes may reflect any combination of altered synapse count, structure or density.

All ten visual processing neurons we studied have significantly altered synapse counts in *trpγ* mutants (Fig. 3). Notably, these changes are cell-type- and domain-specific. For example, the synaptic output domains of Mi1—in medulla layers M1, M5 and M9–10—are differentially affected, with the largest decrease in synapse counts occurring in M9–10 (Fig. 3a–c). By contrast, in L4 and L5, the relative synapse count drops are comparable in each layer (Extended Data Fig. 3d, e). Further, in one cell type, Tm9, synapse counts increase in the mutant (Fig. 3d, Extended Data Fig. 3g). We conclude that *Trpγ* is necessary for establishing the stereotyped, cell-type-specific synaptic structure of the *Drosophila* visual system.

For two cell types, Dm9 and Tm9, we combined STaR analysis with $Trp\gamma^{G4}$-driven Trpγ-D and found that expression of a single copy of this

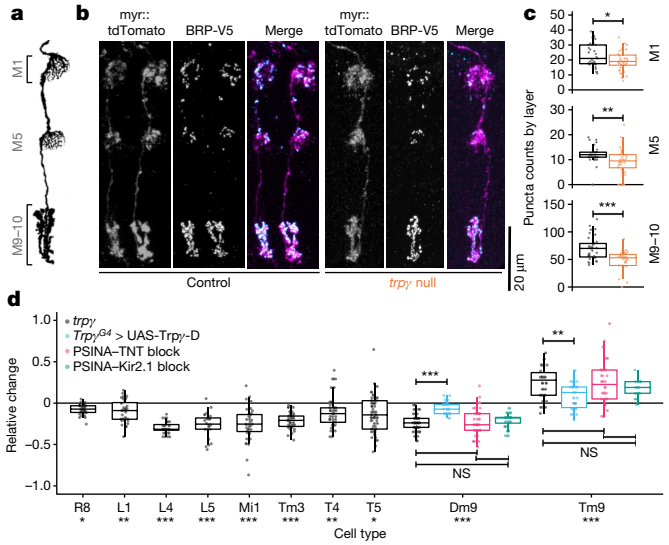

Fig. 3 | Synapse formation in the visual system depends on PSINA. **a**, Schematic of Mi1, with processes in medulla layers M1, M5 and M9–10 (adapted from ref. [41]). **b**, Micrographs of Mi1 neurons in control (left set) and *trpγ* (right set) flies with cell membranes (myr::tdTomato, magenta in merged) and presynaptic sites (BRP-V5, cyan in merged) labelled. Scale bar, 20 µm. **c**, Mi1 Brp puncta counts by layer in heterozygous control (black, $n = 35$ cells) and *trpγ* (orange, $n = 36$ cells) flies. Each data point shows the number of Brp puncta counted in the arborization of one Mi1 neuron in one of three medulla layers. Box-and-whiskers mark 5th, 25th, 50th, 75th and 95th percentiles. $^*P < 0.05$; $^{**}P < 0.01$; $^{***}P < 0.001$ by Welch's *t*-test following Shapiro–Wilk test. **d**, Cell-type-specific Brp puncta counts in *trpγ* mutants (black, $n = 26$–65 cells per cell type), in the *trpγ*, $Trpγ^{G4}$> UAS-Trpγ-D rescue condition (cyan, $n = 24$ cells for Dm9, $n = 30$ cells for Tm9), in flies expressing TNT (magenta, $n = 43$ cells for Dm9, $n = 35$ cells for Tm9) or Kir2.1 (green, $n = 40$ for Dm9, $n = 25$ for Tm9) pan-neuronally displayed as change relative to control averages ($n = 18$–61 cells per cell type), calculated by dividing raw Brp counts in the mutant set by the average of the corresponding control set and subtracting 1 from each new ratio value. Data displayed as in **c**. Asterisks below cell type names report tests of *trpγ* mutants versus control. $^*P < 0.05$; $^{**}P < 0.01$; $^{***}P < 0.001$ by Welch's *t*-test following Shapiro–Wilk test or Tukey's post hoc test following ANOVA for multiple groups.

transgene in Trpγ+ cells significantly rescues the synaptic phenotypes (Fig. 3d, Extended Data Fig. 3h). Our genetic scheme included GAL80 expression specifically in Dm9 or Tm9, so that GAL4-driven Trpγ-D expression would be inhibited in these cell types. Thus, these results are also consistent with a non-cell-autonomous requirement for *Trpγ*.

To follow up on cell autonomy, we performed mosaic analysis with a repressible cell marker (MARCM)[24] in combination with STaR to label pre-synaptic sites of *trpγ* mutant clones on a wild-type background. We focused on L5, which expresses *Trpγ* during development[25]. There is no significant difference in synapse counts between mutant and wild-type clones (Extended Data Fig. 3i), indicating that the L5 *trpγ* synaptic phenotype is not due to a cell-autonomous requirement for this gene.

If the *trpγ* synaptic phenotypes are due to attenuation of PSINA, then a more severe perturbation of developmental activity should also affect synapse formation. To this end, we expressed either the inward rectifying potassium channel and neuronal inhibitor Kir2.1[26] or tetanus toxin (TNT) pan-neuronally during the second half of pupal development and assessed synaptic structure with STaR in Dm9 and Tm9 cells. Pan-neuronal Kir2.1 or TNT expression effectively suppressed PSINA (Fig. 5a–c, Extended Data Fig. 9d, e), and the resulting changes in synapse counts were indistinguishable from the *trpγ* phenotypes (Fig. 3d). These results indicate that the synaptic defects are caused by the attenuation of PSINA in *trpγ* mutants. Additionally, the alteration of cell-type-specific PSINA dynamics is as severe a perturbation to synaptic development as the loss of nearly all developmental activity.

The specificity of the Tm9 driver[27] made it possible to compare the time course of synaptic development with and without PSINA. Synapse counts under these two conditions are comparable at 60 hAPF, begin diverging at 72 hAPF, and reach their respective adult complements at 84 hAPF (Extended Data Fig. 3g, j). The wild-type trend is consistent with previous studies[12,13], and the similarly monotonic increase in the absence of PSINA suggests that developmental activity acts to influence a default synaptogenesis program.

Trpγ+ activity is the template for PSINA

The correspondence of synaptic defects seen with pan-neuronal inhibition and the *trpγ* mutation as well as the non-autonomous origin of the mutant phenotypes shifted our attention from the gene to the expression domain. From 24 to 72 hAPF, $Trpγ^{G4}$ labels an increasing number of cells in the brain (Fig. 4a, Extended Data Fig. 4a). The half-brain count peaks at 1,095 ± 105 at 72 hAPF; by eclosion this figure is reduced by 40%. Throughout pupal development, the majority of Trpγ+ cells are found in the central brain, with optic lobes accounting for at most 25% of all Trpγ+ cells and 8% of the strongly labelled Trpγ+ cells (Fig. 4a, Extended Data Fig. 4a).

We characterized the Trpγ expression domain at 72 hAPF with immunofluorescence. A comparison of the neuronal anti-elav and glial anti-repo staining revealed that Trpγ+ cells are neurons (Extended Data Fig. 4b, c). Consistent with this, we found that RNAi-mediated Trpγ knockdown in neurons produces to a PSINA phenotype similar to that of the whole-animal mutant, whereas the knockdown in glia has no effect (Extended Data Fig. 4d, e). Trpγ+ neurons are a diverse group that includes cholinergic, glutamatergic, GABAergic (γ-aminobutyric acid-producing), serotonergic and dopaminergic cells (Extended Data Fig. 5a–e). The expression domain also contains DH31, DH44, Pdf and SIFamide producing neuropeptide cells (Extended Data Fig. 5f–i).

Trpγ+ neuronal processes cover all regions of the developing brain in apparent space-filling fashion (Fig. 4b). We aimed to visualize individual neuronal morphologies. FLP recombinase-mediated approaches resulted in high density labelling independent of imposed controls on recombinase activity. Thus, we generated a new series of reagents, SPARC3-Out-GAL80, based on the recent sparse predictive activity through recombinase competition (SPARC) approach to sparse labelling[28] (Extended Data Fig. 6a–d, Supplementary Discussion). Using SPARC3-Out-GAL80 in series with UAS-SPARC2-LexA to control $Trpγ^{G4}$ output, we reduced the labelling density from approximately 2,000 to around 5 to 10 neurons per brain, making it possible to discern morphologies of individual Trpγ+ cells. This effort revealed a number of visual processing neurons, including ones (for example, lamina neurons) that have been reported to express *Trpγ* during development[25] (Extended Data Fig. 6f). We also observed a number of less familiar neurons that innervate the visual system from the central brain (Fig. 4c, Extended Data Fig. 6e, g), suggesting possible structural origins to the non-autonomous *trpγ* phenotypes.

The fly brain comprises some 150,000 neurons[29]; Trpγ is expressed in <2% of this complement. To compare pan-neuronal PSINA to the activity in Trpγ+ neurons, we performed two-colour calcium imaging[30] (Fig. 4d). In both wild type and *trpγ* mutants, PSINA is highly correlated between Trpγ+ neurons and neurons labelled by the nSyb-derived 57C10 enhancer fragment (Fig. 4e). Additionally, the mutation causes the same loss of amplitude in Trpγ+ neurons as it does for all neurons (Fig. 4f, compare with Fig. 1e). With the greater sensitivity of two-photon microscopy, we found that the *trpγ* mutation also leads to an increased sweep count in Trpγ+ neurons (Fig. 4g, h, Supplementary Video 3). Notably, Trpγ+ morphologies visible by two-photon microscopy were dominated by wide-field processes reminiscent of innervating neurons observed with sparse labelling (Fig. 4g). Together, these results suggest that the approximately 2,000 Trpγ+ neurons provide the immediate template for pan-neuronal PSINA.

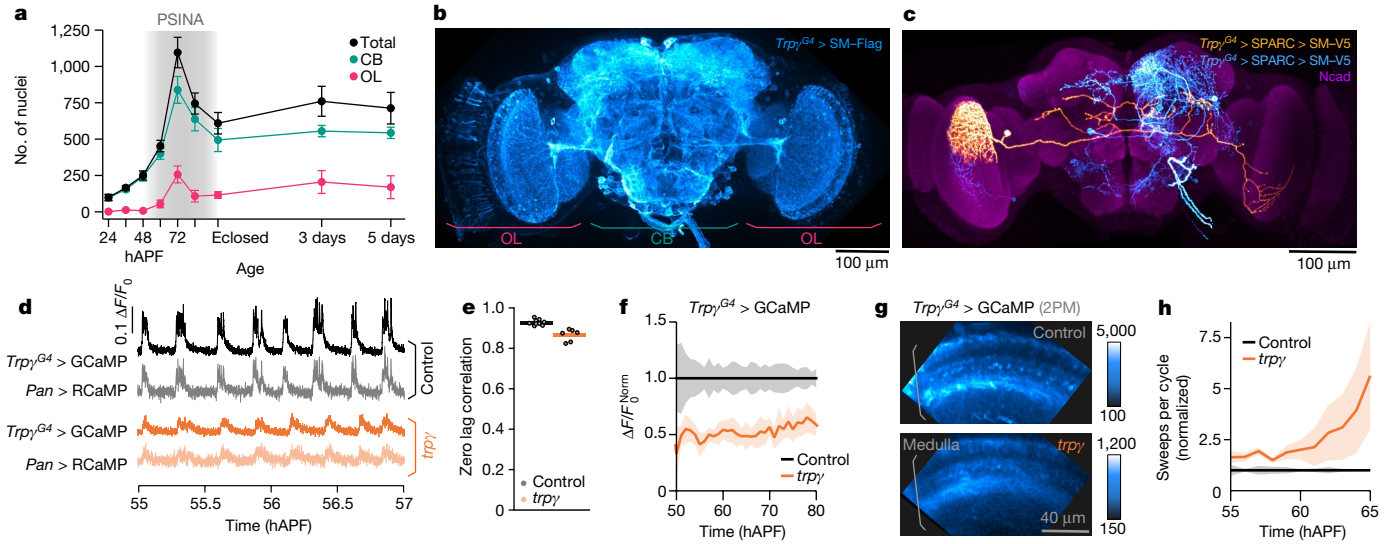

Fig. 4 | Trpγ+ neurons are the template for brain-wide PSINA. a, Half-brain Trpγ+ nuclei counts over time. OL, optic lobe. Error bars show s.d. $n = 3–8$ brains per time point. **b**, Coverage of the 72 hAPF brain by *Trpγ*+ neurons expressing myr::SM-Flag. Most *Trpγ*+ neurons are labelled; some sparseness was introduced using FLP-Out to improve staining. Image maximum intensity projection (MIP) of confocal stack. Scale bar, 100 µm. **c**, Single *Trpγ*+ neuron (orange, manually segmented) in the context of others (cyan) labelled using SPARC. Neurons expressing myr::SM-V5. Reference marker (magenta), Ncad. Image MIP of three stitched confocal stacks of 72 hAPF brain. Scale bar, 100 µm. **d**, PSINA traces in control (top two, grayscale) and *trpγ* (bottom two, orange) pupae, recorded from co-expressed GCaMP6s in Trpγ+ neurons (darker hues) and pan-neuronal RCaMP1b (lighter hues). Traces acquired with wide-field imaging. **e**, Zero-lag correlation of PSINA in Trpγ+ and pan-neuronal expression domains. Round markers show a single time series; bars show genotype average. $n = 9$ control flies; $n = 6$ *trpγ* flies. **f**, Active phase average amplitude recorded in Trpγ+ neurons binned by hour and normalized to control. Shaded areas indicate s.d. $n = 9$ control flies, $n = 6$ *trpγ* flies. **g**, Two-photon microscopy AIP of GCaMP6s expressing Trpγ+ processes in the visual system of control (top) and *trpγ* (bottom) pupae at approximately 62 hAPF. Med., Medulla. Scale bar, 40 µm. **h**, Sweeps per cycle measured in two-photon microscopy time series binned by hour and normalized to control. Shaded areas indicate s.d. ($n = 3$ flies for both genotypes).

PSINA requires Trpγ+ neuron activity

To directly test the contribution of activity in Trpγ+ cells to PSINA, we expressed Kir2.1[26] from 40–100 hAPF (that is, during pupal development) and carried out pan-neuronal calcium imaging (Fig. 5a–c, Extended Data Fig. 7a–d).

Silencing Trpγ+ neurons severely attenuates PSINA at a level similar to pan-neuronal expression of Kir2.1 (Fig. 5b, c, Supplementary Video 4). The extent of attenuation cannot be explained simply by a loss of Trpγ+ neuron activity, which contributes about 15% of the total PSINA signal amplitude (Extended Data Fig. 7e, f). Wide-field imaging reveals residual cycles with fewer sweeps, shorter active phases and perturbed periodicity (Fig. 5c, Extended Data Fig. 7a). This residual activity remains coordinated throughout the brain (Extended Data Fig. 7g–j). With two-photon microscopy in the visual system, the reduced cycles are evident with both Trpγ+ and pan-neuronal silencing and, in both cases, only distinct layers in the distal medulla become active (Extended Data Fig. 7b–d). The marked effect of driving Kir2.1 with *Trpγ*^{G4} indicates that the neurons that shape the spatiotemporal structure of PSINA reside in the *Trpγ* expression domain.

To test whether targeted silencing of Trpγ+ neurons also affects synaptic development, we expressed Kir2.1 in the Trpγ+ domain during the second half of pupal development and assessed synaptic structure with STaR in Dm9 and Tm9 cells. Both cell types show altered Brp counts that are indistinguishable from what we observe with pan-neuronal silencing using Kir2.1 (Extended Data Fig. 7k), indicating that pan-neuronal activity driven by Trpγ+ neurons influences synaptogenesis.

Specifically silencing Trpγ+ neurons in the central brain, but not in the optic lobes, attenuates PSINA across the brain (Extended Data Fig. 8). Notably, the converse experiment has no significant effect, even in the optic lobes where Trpγ+ neurons are made to express Kir2.1 (Extended Data Fig. 8). These results are consistent with the non cell-autonomous origin of the visual system *trpγ* synaptic phenotypes and, together with the Trpγ+ neurons that bridge the central brain and the optic lobes, suggest that Trpγ+ neurons carry or relay PSINA into the visual system.

Additional perturbations of the Trpγ+ domain also lead to PSINA attenuation. Ablating Trpγ+ neurons during PSINA results in loss of PSINA comparable to Kir2.1 silencing (Extended Data Fig. 9b, c). TNT expression in Trpγ+ neurons also attenuates PSINA (Extended Data Fig. 9d, e). Although it is the least potent of the three perturbations, TNT is still much more effective at inhibiting PSINA when expressed in the approximately 2,000 Trpγ+ neurons than in other neuronal populations: expressing TNT in aminergic, glutamatergic or GABAergic neurons has no significant effect on PSINA (Extended Data Fig. 9f). We conclude that the results of Trpγ+ silencing cannot be explained by the silencing of an arbitrary subpopulation of neurons.

For a complementary gain-of-function approach, we used the thermogenetic neuronal activator TrpA1[31]. Activating TrpA1 pan-neuronally leads to sustained high frequency, low amplitude events that sit on an elevated plateau of GCaMP fluorescence, consistent with constitutive contributions from spiking and non-spiking neurons (Fig. 5d–f, Extended Data Fig. 10a, b). TrpA1-mediated activation of Trpγ+ neurons produces an uninterrupted train of sweeps similar in amplitude to that in controls, but which lack the periodic structure of wild-type PSINA (Fig. 5d–f, Extended Data Fig. 10a, b). By contrast, TrpA1-mediated activation of GABAergic or glutamatergic neurons does not alter the temporal structure of wild-type PSINA (Extended Data Fig. 10c, d). Notably, whereas pan-neuronal activation stimulates brain-wide responses as early as 36 hAPF, Trpγ+ neurons become effective drivers of stimulated activity starting at 48 hAPF, coincident with the onset of PSINA (Fig. 5e). These results are consistent with the notion that Trpγ+ neurons can trigger brain-wide spiking activity during PSINA.

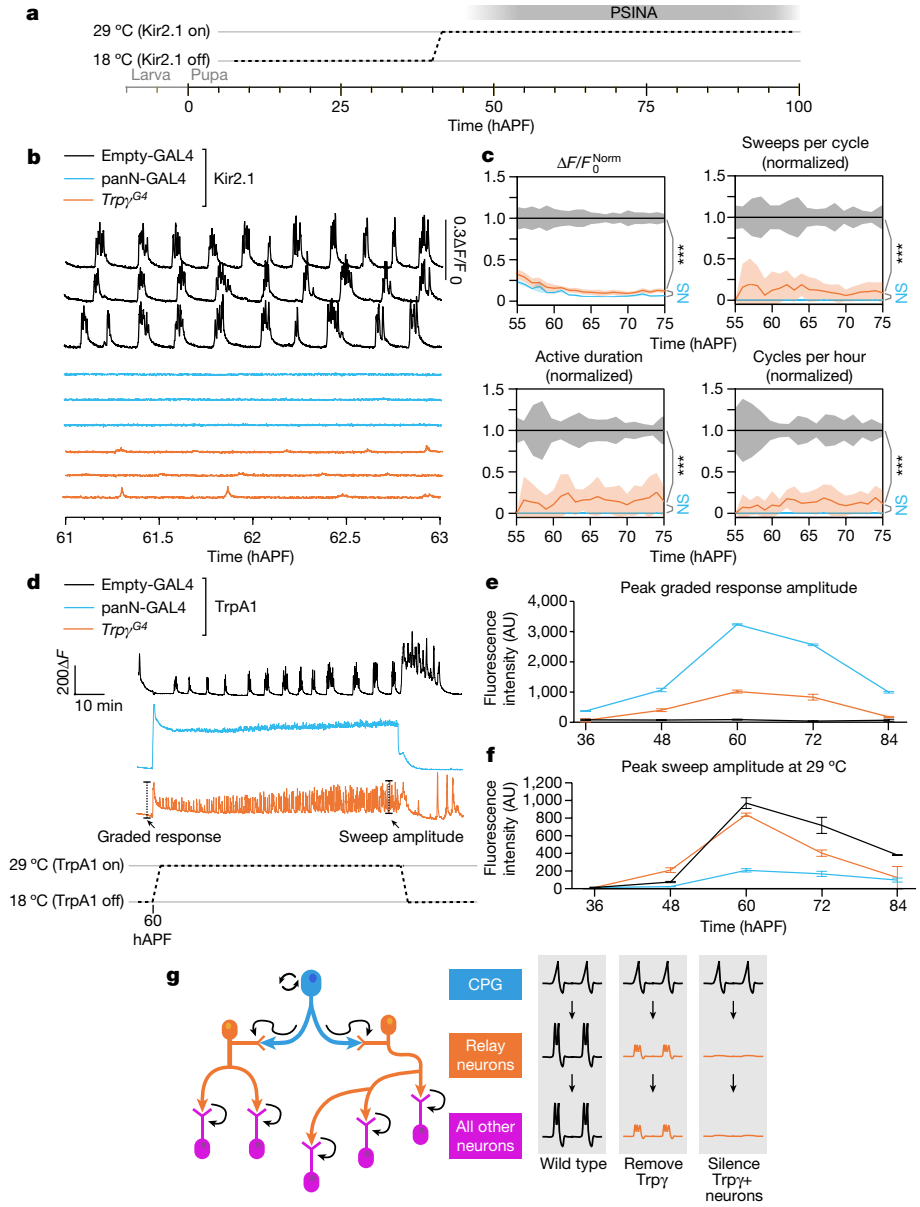

Fig. 5 | PSINA requires Trpγ+ neuron activity. a, Expression control of UAS-Kir2.1 with TARGET; flies were shifted from 18 °C to 29 °C at 40 hAPF. **b**, **c**, PSINA traces from pan-neuronal GCaMP6s (**b**) and active phase average amplitude (top left), sweeps per cycle (top right), active phase duration (bottom left) and cycles per hour (bottom right), binned by hour and normalized to control (**c**) in control (empty-GAL4, black, $n = 7$ flies), panN-GAL4>Kir2.1 (blue, $n = 7$ flies) and $Trpγ^{G4}$>Kir2.1 (orange, $n = 9$ flies) pupae. Shaded areas indicate s.d. $^{***}P < 0.001$ by Welch's *t*-test following Shapiro–Wilk test versus $Trpγ^{G4}$>Kir2.1 activity at 60 hAPF. **d**, Activity from pan-neuronal GCaMP6s in control (empty-GAL4, black), panN-GAL4>TrpA1 (blue) and $Trpγ^{G4}$>TrpA1 (orange) pupae at 60 hAPF. Pupae were reared at 18 °C and shifted to 29 °C. Initial graded response to temperature shift and maximum sweep amplitude are marked. **e**, **f**, Peak graded response to temperature shift (**e**) and peak sweep amplitude at 29 °C (**f**). Error bars show s.d. $n = 2$–4 flies per time point and condition. Genotypes are colour matched to those in **d**. **g**, Intrinsically active CPG neurons (cyan) activate Trpγ+ relay neurons (orange), which, in turn, activate all other neurons (magenta) in specific spatiotemporal patterns. When relay activity is attenuated or silenced, all downstream neurons are similarly affected.

Discussion

We report that perturbing PSINA leads to cell-type-specific changes to synaptic structure in the fly visual system (Fig. 3d). We see the same changes with both the near-complete block of PSINA with pan-neuronal TNT or Kir2.1 and the attenuated and altered activity due to loss of *Trpγ*, suggesting that wild-type synaptic development requires the stereotyped activity patterns of PSINA. This, together with the observations that synapses still form without activity (Fig. 3d) and that activity across the brain is templated by a discrete population of neurons (Fig. 4d–f), is consistent with an instructive role for PSINA. The genetic access offered by the *Trpγ*+ domain to the origins of the patterns—that is, the information content—of PSINA promises a more rigorous test of this putative instructive role[32] in the future.

The synaptic changes due to altered PSINA are comparable to recent findings that used electron microscopy reconstructions to compare the effects of cell-type-specific perturbations to wiring in the developing larval nervous system[33]. This study found that silencing a mechanosensory neuron during development reduced the number of pre-synaptic sites and changed the relative strength of connections to post-synaptic partners. These changes produced

altered behavioural responses, indicating that quantitatively modest perturbations of synaptic structure can significantly alter circuit function and output.

Trpγ is a non-selective cation channel in the classical TRP (TRPC) subfamily of TRP channel super-family[19]. It can interact with the other two fly TRPCs[19], TrpL and Trp. Constitutive loss of *Trpγ* results in coordination and fine motor control deficits, due to a requirement for the channel in proprioceptive organs of the adult[17]. Here, we show that expression of *Trpγ* in around 2,000 neurons in the developing brain is necessary and sufficient for wild-type PSINA (Fig. 1). Future studies will be required to characterize the behavioural consequences of developmental loss of *Trpγ* from the brain, or of other disruptions to PSINA.

The importance of the *Trpγ* expression domain to PSINA is underscored by two results: (1) silencing Trpγ+ neurons results in activity inhibition similar to pan-neuronal silencing (Fig. 5b, c); and (2) pan-neuronal activity phenocopies the cell-autonomous *trpγ* phenotype—that is, loss of *trpγ* has the same effect on activity across the whole brain as it does in Trpγ+ neurons (Fig. 4d–f). Together, these indicate that Trpγ+ neurons both relay PSINA across the brain and form an activity scaffold that templates the spatiotemporal patterns of PSINA (Fig. 5g, Extended Data Fig. 10e). We hypothesize that cell-type-specific PSINA dynamics are shaped by the activity patterns of upstream Trpγ+ relay neurons.

Residual rhythmic activity persists with both pan-neuronal and Trpγ+ silencing (Fig. 5b, Extended Data Fig. 7b–d), revealing the presence of a PSINA central pattern generator (CPG) that is outside the reach of these manipulations (Supplementary Discussion). Consistent with previously described CPGs[34], PSINA arises independent of sensory input[3] and its temporal patterns are temperature sensitive (Extended Data Fig. 10a, b). Although some Trpγ+ neurons may contribute to this CPG, the overall picture that emerges for PSINA is that of a hierarchical cascade, with a CPG triggering a small set of Trpγ+ relay neurons, which subsequently activate the rest of the brain in specific spatiotemporal patterns (Fig. 5g, Extended Data Fig. 10e). A more derived mechanism could involve a network of distinct CPGs synchronized via feedback, with Trpγ+ neurons acting downstream of each CPG to propagate activity throughout the brain (Extended Data Fig. 10e).

The dynamic expression domain of *Trpγ*, peaking at a cell count of approximately 2,000 at 72 hAPF and contracting thereafter, suggests that the PSINA relay may be a functionally or structurally transient feature. Transient populations have been documented in mammalian models of developmental activity, including the Kölliker's organ in the cochlea and sub-plate and Cajal–Retzius neurons in the neocortex[35–37]. The existence of temporally dedicated neurons supports the notion that developmental activity is a hardwired phase of nervous system development. Evidence for transient neuronal populations in the developing fly brain[38], including PDF-TRI cells[39], which are Trpγ+ neurons (Extended Data Fig. 5g), raises the possibility of a population of neurons that exist only during pupal development to coordinate PSINA.

Consistent with their role as a relay system, the processes of Trpγ+ neurons occupy every region of the fly brain (Fig. 4b). In the optic lobes, the Trpγ+ domain is represented by both resident visual processing neurons and by expansive processes originating from the central brain (Fig. 4c, Extended Data Fig. 6e–g). The *trpγ* synapse and activity phenotypes are due to loss of function outside the visual system (Fig. 3d, Extended Data Fig. 8), suggesting that the subset of Trpγ+ neurons with long range projections are responsible for relaying PSINA across the brain.

In many mammalian models of developmental activity, local circuitry initiates activity[1]. Although initiation and patterning of activity may be local, the high degree of inter-connectivity in the adult brain does suggest the feasibility of coordination at a larger scale. Indeed, activity in the retina is relayed out to higher visual centres by retinal ganglion cells[6]. Here, the more approachable scale of the fly nervous system reveals that it is possible to coordinate developmental activity across the whole brain. Studies of brain-wide, low-frequency activity in the adult[40] suggest that the neuronal infrastructure for such long-range coordination exists in mammals; it remains to be seen whether similar infrastructure is used during development.

In summary, here we identify a brain-wide relay system to produce PSINA, which—in turn—influences synaptogenesis. The structure and connectivity of this relay circuit will be critical for understanding how brain-wide developmental activity is generated. A mechanistic description of developmental activity will be necessary to address how and to what extent such activity represents a fundamental ingredient in the recipe for building a brain.

Online content

Any methods, additional references, Nature Research reporting summaries, source data, extended data, supplementary information, acknowledgements, peer review information; details of author contributions and competing interests; and statements of data and code availability are available at https://doi.org/10.1038/s41586-022-04406-9.

1. Blankenship, A. G. & Feller, M. B. Mechanisms underlying spontaneous patterned activity in developing neural circuits. *Nat. Rev. Neurosci.* **11**, 18–29 (2010).
2. Ackman, J. B. & Crair, M. C. Role of emergent neural activity in visual map development. *Curr. Opin. Neurobiol.* **24**, 166–175 (2014).
3. Akin, O., Bajar, B. T., Keles, M. F., Frye, M. A. & Zipursky, S. L. Cell-type-specific patterned stimulus-independent neuronal activity in the *Drosophila* visual system during synapse formation. *Neuron* **101**, 894–904.e5 (2019).
4. Galli, L. & Maffei, L. Spontaneous impulse activity of rat retinal ganglion cells in prenatal life. *Science* **242**, 90–91 (1988).
5. Meister, M., Wong, R. O., Baylor, D. A. & Shatz, C. J. Synchronous bursts of action potentials in ganglion cells of the developing mammalian retina. *Science* **252**, 939–943 (1991).
6. Ackman, J. B., Burbridge, T. J. & Crair, M. C. Retinal waves coordinate patterned activity throughout the developing visual system. *Nature* **490**, 219–225 (2012).
7. Bansal, A. et al. Mice lacking specific nicotinic acetylcholine receptor subunits exhibit dramatically altered spontaneous activity patterns and reveal a limited role for retinal waves in forming ON and OFF circuits in the inner retina. *J. Neurosci.* **20**, 7672–7681 (2000).
8. Burbridge, T. J. et al. Visual circuit development requires patterned activity mediated by retinal acetylcholine receptors. *Neuron* **84**, 1049–1064 (2014).
9. McLaughlin, T., Hindges, R. & O'Leary, D. D. Regulation of axial patterning of the retina and its topographic mapping in the brain. *Curr. Opin. Neurobiol.* **13**, 57–69 (2003).
10. Sugie, A., Marchetti, G. & Tavosanis, G. Structural aspects of plasticity in the nervous system of *Drosophila*. *Neural Dev.* **13**, 14 (2018).
11. Hiesinger, P. R. et al. Activity-independent prespecification of synaptic partners in the visual map of *Drosophila*. *Curr. Biol.* **16**, 1835–1843 (2006).
12. Chen, Y. et al. Cell-type-specific labeling of synapses in vivo through synaptic tagging with recombination. *Neuron* **81**, 280–293 (2014).
13. Muthukumar, A. K., Stork, T. & Freeman, M. R. Activity-dependent regulation of astrocyte GAT levels during synaptogenesis. *Nat. Neurosci.* **17**, 1340–1350 (2014).
14. Takemura, S. Y. et al. A visual motion detection circuit suggested by *Drosophila* connectomics. *Nature* **500**, 175–181 (2013).
15. Venkatachalam, K. & Montell, C. TRP channels. *Annu. Rev. Biochem.* **76**, 387–417 (2007).
16. Chen, T. W. et al. Ultrasensitive fluorescent proteins for imaging neuronal activity. *Nature* **499**, 295–300 (2013).
17. Akitake, B. et al. Coordination and fine motor control depend on *Drosophila* TRPγ. *Nat. Commun.* **6**, 7288 (2015).
18. Kanca, O. et al. An efficient CRISPR-based strategy to insert small and large fragments of DNA using short homology arms. *eLife* **8**, e51539 (2019).
19. Xu, X. Z., Chien, F., Butler, A., Salkoff, L. & Montell, C. TRPγ, a drosophila TRP-related subunit, forms a regulated cation channel with TRPL. *Neuron* **26**, 647–657 (2000).
20. Batut, P. & Gingeras, T. R. RAMPAGE: promoter activity profiling by paired-end sequencing of 5′-complete cDNAs. *Curr. Protoc. Mol. Biol.* **104**, Unit 25B.11 (2013).
21. McGuire, S. E., Le, P. T., Osborn, A. J., Matsumoto, K. & Davis, R. L. Spatiotemporal rescue of memory dysfunction in *Drosophila*. *Science* **302**, 1765–1768 (2003).
22. Akin, O. & Zipursky, S. L. Frazzled promotes growth cone attachment at the source of a Netrin gradient in the. *eLife* **5**, e20762 (2016).
23. Takemura, S. Y., Lu, Z. & Meinertzhagen, I. A. Synaptic circuits of the *Drosophila* optic lobe: the input terminals to the medulla. *J. Comp. Neurol.* **509**, 493–513 (2008).
24. Lee, T. & Luo, L. Mosaic analysis with a repressible cell marker for studies of gene function in neuronal morphogenesis. *Neuron* **22**, 451–461 (1999).
25. Kurmangaliyev, Y. Z., Yoo, J., Valdes-Aleman, J., Sanfilippo, P. & Zipursky, S. L. Transcriptional programs of circuit assembly in the *Drosophila* visual system. *Neuron* **108**, 1045–1057.e6 (2020).
26. Baines, R. A., Uhler, J. P., Thompson, A., Sweeney, S. T. & Bate, M. Altered electrical properties in *Drosophila* neurons developing without synaptic transmission. *J. Neurosci.* **21**, 1523–1531 (2001).
27. Peng, J. et al. *Drosophila* Fezf coordinates laminar-specific connectivity through cell-intrinsic and cell-extrinsic mechanisms. *eLife* **7**, e33962 (2018).
28. Isaacman-Beck, J. et al. SPARC enables genetic manipulation of precise proportions of cells. *Nat. Neurosci.* **23**, 1168–1175 (2020).
29. Chiang, A. S. et al. Three-dimensional reconstruction of brain-wide wiring networks in *Drosophila* at single-cell resolution. *Curr. Biol.* **21**, 1–11 (2011).

30. Dana, H. et al. Sensitive red protein calcium indicators for imaging neural activity. *eLife* **5**, e12727 (2016).
31. Pulver, S. R., Pashkovski, S. L., Hornstein, N. J., Garrity, P. A. & Griffith, L. C. Temporal dynamics of neuronal activation by channelrhodopsin-2 and TRPA1 determine behavioral output in *Drosophila* larvae. *J. Neurophysiol.* **101**, 3075–3088 (2009).
32. Crair, M. C. Neuronal activity during development: permissive or instructive. *Curr. Opin. Neurobiol.* **9**, 88–93 (1999).
33. Valdes-Aleman, J. et al. Comparative connectomics reveals how partner identity, location, and activity specify synaptic connectivity in *Drosophila*. *Neuron* **109**, 105–122.e7 (2021).
34. Mulloney, B. & Smarandache, C. Fifty years of CPGs: two neuroethological papers that shaped the course of neuroscience. *Front. Behav. Neurosci.* **4**, 45 (2010).
35. Tritsch, N. X., Yi, E., Gale, J. E., Glowatzki, E. & Bergles, D. E. The origin of spontaneous activity in the developing auditory system. *Nature* **450**, 50–55 (2007).
36. Wang, H. C. et al. Spontaneous activity of cochlear hair cells triggered by fluid secretion mechanism in adjacent support cells. *Cell* **163**, 1348–1359 (2015).
37. Luhmann, H. J. et al. Spontaneous neuronal activity in developing neocortical networks: from single cells to large-scale interactions. *Front. Neural Circuits* **10**, 40 (2016).
38. Özel, M. N. et al. Neuronal diversity and convergence in a visual system developmental atlas. *Nature* **589**, 88–95 (2021).
39. Helfrich-Förster, C. Development of pigment-dispersing hormone-immunoreactive neurons in the nervous system of *Drosophila melanogaster*. *J. Comp. Neurol.* **380**, 335–354 (1997).
40. Leong, A. T. et al. Long-range projections coordinate distributed brain-wide neural activity with a specific spatiotemporal profile. *Proc. Natl Acad. Sci. USA* **113**, E8306–E8315 (2016).
41. Fischbach, K. F. & Dittrich, A. P. M. The optic lobe of *Drosophila melanogaster*. 1. A Golgi analysis of wild-type structure. *Cell Tissue Res.* **258**, 441–475 (1989).

Methods

Experimental model and subject details

Flies were reared at 18 °C, 25 °C, or 29 °C on standard cornmeal/molasses medium; developmental time was matched to the 25 °C standard (1×) using relative rates of 0.5× and 1.25× for 18 °C and 29 °C, respectively[42]. Pupal development was staged with respect to white pre-pupa formation (w.p.p., 0 h APF) or head eversion (h.e., 12 hAPF). GAL4/UAS and LexA/LexAop expression systems[43,44] were used to drive cell-type-specific transgene expression. Complete genotypes used in each experiment can be found in Supplementary Table 1.

Lifespan assay

The protocol was adapted from ref. [45]. In brief, 1-day-old flies from a 24-h egg-lay were flipped into fresh bottles and allowed to mate for 2 days. Fifty males and females of each genotype (wild type (WT) and *trpγ* nulls) were moved to vials at a density of 10 flies per vial. Vials were stored horizontally at 25 °C and 75% relative humidity with 12:12 h light:dark cycles. Flies were flipped into fresh (less than one week old) vials every 2–3 days; deaths and censors (that is, flies lost during transfer) were scored during each transfer until there were no survivors. Assay was carried out in two technical replicates, separated by a day in their start time.

Generation of UAS-Trpγ-AB and UAS-Trpγ-D transgenic lines

See Supplementary Table 2 for primers used to PCR amplify the Trpγ coding sequence from pcDNA3-Trpγ[17]. We subcloned the fragments between the NotI and the XbaI sites of pJFRC165. Note that in our Trpγ-D open reading frame, the non-canonical start codon CTG is converted to ATG to ensure robust GAL4-driven expression. After sequence-verifying the new plasmids, we introduced UAS-Trpγ-AB or -D DNA into y[1] w[*]; P{y[+t7.7]=CaryIP}su(Hw)attP1 embryos via phiC31 integrase-mediated germline transformation (BestGene).

Generation SPARC3-Out-GAL80 flies

All plasmids were generated through synthesis and molecular cloning by Genscript; see Supplementary Table 3 for details.

gRNA-targeting vector. Supplementary Table 4 provides the gRNA sequences used in the design of pCFD5-U6-3-t-Su(Hw)attP5[28].

αTub84B-SPARC3 CRISPR donor synthesis. To generate CRISPR donor plasmids targeting sequences near Su(Hw)attP5, we defined homology arms directly adjacent to the gRNA targets defined above. For the region near Su(Hw)attP5, we defined a 1,044 bp left homology arm (2R: 14304046..14305089) and a 1,044 bp right homology arm (2R:14305090..14306133). We designed these homology arms to fully recapitulate genomic DNA after CRISPR-HDR by overlapping the gRNA target sites and mutating the proximal adjacent motifs (PAMs) of gRNA targets. Genscript synthesized these homology arms and cloned them into pHD-3xP3-dsRed-ΔattP[28] using AarI for left homology arms and Sap-I for right homology arms to generate pHD-3XP3-dsRed-ΔattP-CRISPR-donor-Su(Hw)attP5.

Next, the SPARC3-OUT-D-GAL80 module was synthesized by Genscript and cloned into the unique Kpn-I site of either pHD-3XP3-dsRed-ΔattP-CRISPR-donor-Su(Hw)attP5 to generate pHD-SPARC3-OUT-D-GAL80-Su(Hw)attP5. Then Genscript PCR amplified the αTub84B promoter[24] from pJFRC-αTub84B-IVS-PhiC31[28] and cloned it into pHD-SPARC3-OUT-D-GAL80-Su(Hw)attP5 to generate pHD-αTub84B-SPARC3-OUT-D-GAL80-Su(Hw)attP5. Genscript next synthesized attP38 and attP34 fragments[28] and cloned them into pHD-αTub84B-SPARC3-OUT-D-GAL80-Su(Hw)attP5 via Stu-I and Asc-I sites to generate pHD-αTub84B-SPARC3-OUT-I-GAL80-Su(Hw)attP5 and pHD-αTub84B-SPARC3-OUT-S-GAL80-Su(Hw)attP5 respectively.

For detailed construct maps of αTub84B-SPARC3-OUT, see Extended Data Fig. 6a–d.

Generation of transgenic flies. αTub84B-SPARC3-OUT-GAL80 transgenic flies were generated by Bestgene using standard construct injections and CRISPR-HDR. Transformants were identified by the marker 3xP3-DsRed. The three fly lines (that is, D, I and S variants) are available upon request.

Wide-field imaging

Pupae were staged for w.p.p. formation or h.e. and reared at 25 °C unless otherwise noted. The cuticle around the head was removed with fine forceps and the flies were fixed to a metal plate (McMaster-Carr) with double-sided adhesive tape (3M). The metal plate was placed in a custom environmental chamber to maintain temperature and humidity. This chamber comprised: a PTC1 temperature-controlled breadboard (Thorlabs) to maintain sample temperature at 18 °C, 25 °C or 29 °C; a set of four 35-mm dishes filled with deionized water to maintain humidity; and a 150-mm petri-dish lid to provide enclosure. To improve imaging quality, a large format coverslip was fitted into a rectangular opening made in the lid. This coverslip sat in the optical path, between the pupae and the objective lens, and was treated with Barbasol shaving cream (Perio) to prevent condensation during temperature shifts.

Images were captured using an Axio Zoom.V16 epifluorescence microscope (Zeiss) equipped with a Retiga R1 CCD Camera (QImaging) and X-Cite TURBO LED 6-Channel Light Source (Excelitas Technologies). Images were acquired at 0.4 Hz with a PlanNeoFluar Z 1X objective (Zeiss) with 100 ms exposure time for green fluorophores and 500 ms exposure time for red fluorophores. Acquisition was controlled by Slidebook 6 software (Intelligent Imaging). Time series were processed with Fiji[46] and analyzed using MATLAB (Mathworks).

Two-photon imaging of the developing visual system

Pupae were prepared for imaging as previously described[22]. In brief, the cuticle around the heads were removed with fine forceps and the flies were attached eye-down on a coverslip coated with a thin layer of embryo glue. A water reservoir on the objective side of the coverglass provided sufficient immersion medium to last through the hours-long imaging sessions; another reservoir below the pupae kept the flies from dehydrating.

Time-lapse imaging of the visual system was performed on a custom-built two-photon microscope[22] with a 20× water immersion objective (Zeiss, W Plan-Apochromat 10x/1.0 DIC) and 2 GaAsP detectors (Hamamatsu). The pupae were kept at 25 °C using an objective heater system (Bioptechs). A tunable Ti:Sapphire pulsed laser (Chameleon Ultra II, Coherent) was used as the light source. GCaMP6s was excited at 940 nm with about 30 mW under-the-objective power. Flies imaged under these conditions developed normally and eclosed on schedule. To observe a thicker cross-section of the visual system than possible with a single optical slice, we used the maximum intensity projection of three successive images taken 2 μm apart in the *z*-axis as the frame for an individual time point. The effective sampling rate of these time series was 0.38 Hz (2.6 s per frame).

Immunofluorescence and confocal microscopy

Brains were dissected in cold Schneider Medium (Gibco 21720–024) and fixed with 3% v/v glyoxal solution (Electron Microscopy Sciences 16525) for 30 min at room temperature or with 4% v/v PFA (Electron Microscopy Sciences 15710) in Schneider Medium for 20 min at room temperature. Brains were then washed out of fixative into PBS (Quality Biological), solubilized in PBST (0.5% Triton-X100 (Sigma T9284) in PBS) for 1 h, and blocked in PBTN (5% Normal Donkey Serum (Jackson ImmunoResearch no. 017-000-121) in PBST) for 1–2 h, all at room temperature. Brains were sequentially incubated in primary and secondary antibodies diluted in PBTN for 24–48 h at 4 °C, with at least 3 washes through PBST over 2 h at room temperature in between and afterwards. Brains were post-fixed with 3% v/v glyoxal for 30 min at room temperature or with 4% v/v PFA in Schneider Medium for 20 min at room temperature, followed by multiple

washes into PBST over 10 min. Brains were finally transferred to Everbrite mounting medium (Biotium 23001) and mounted on to slides for imaging.

Primary antibodies and dilutions used in this study were as follows: mouse monoclonal anti-V5 (Novus Biologicals NBP2-52703–0.2 mg, 1:150), rat monoclonal anti-Flag (DYKDDDDK) (Novus Biologicals NBP1-06712, 1:100), mouse monoclonal anti-c-Myc (Developmental Studies Hybridoma Bank (DSHB) 9E10-concentrate, 1:100), rabbit polyclonal anti-dsRed (Clontech 632496, 1:125), chicken anti-GFP (Abcam ab13970, 1:1,000), rabbit monoclonal anti-HA (Cell Signaling Technology 3724, 1:300), rat monoclonal anti-Ncad (DSHB DN-Ex 8-c, 1:100), mouse monoclonal anti-Elav (DHSB Elav-9F8A9, 1:100), mouse monoclonal anti-Repo (DHSB 8D12 anti-Repo, 1:100), mouse monoclonal anti-Chat (DHSB ChAT4B1, 1:20), mouse monoclonal anti-Pdf (DHSB DF C7, 1:1,000), rabbit polyclonal anti-DVGLUT[47] (1:1,000), rabbit polyclonal anti-DVGAT[48] (1:200), mouse monoclonal anti-TH (Immunostar 22941, 1:200), rabbit polyclonal anti-5-HT (Immunostar 20080, 1:1,000), rabbit polyclonal anti-DH31[49] (1:1,000), rabbit polyclonal anti-DH44[50] (1:1,000) and rabbit polyclonal anti-SIFamide[51] (1:1,000).

Secondary antibodies and dilutions used in this study were as follows: Alexa 488 donkey polyclonal anti-chicken (Jackson ImmunoResearch 703-545-155, 1:400), Alexa 488 donkey polyclonal anti-mouse (Jackson ImmunoResearch 715-545-151, 1:400), Alexa 568 donkey polyclonal anti-rabbit (Invitrogen A10042, 1:400) and Alexa 647 donkey polyclonal anti-rat (Jackson ImmunoResearch 712-605-153, 1:400).

Immunofluorescence images were acquired using Zeiss LSM 780 confocal microscope with 20×/0.8 air, 40×/1.4 oil immersion or 40×/1.2 glycerol immersion objectives (Zeiss).

Analysis of two-photon imaging data

Analysis was carried out as previously described[3].

Analysis of pupal wide-field imaging data

Preparation of time lapse imaging data was performed in Fiji (ImageJ). Per frame pixel averages of user-defined ROIs were used to define raw signal (F) traces from the image time series. The raw signal was baseline subtracted and the resulting net signal (ΔF) was used in subsequent analysis, performed in MATLAB. $\Delta F/F_0$ is defined as the baseline-subtracted net signal divided by the raw baseline signal.

For each time series, sweeps were defined by growing the 'domain' of each signal local maximum (that is, peak) through preceding and succeeding time-points until another peak at least 75% as large as the original was reached in both directions. Ordered signal peaks were processed iteratively in this fashion, starting from the largest on down, and lesser peaks which were subsumed in the sweep domain of a larger one were removed from separate evaluation. Clusters of sweeps were used to define active phases; silent phases were defined by the span between active phases; cycles were defined as the sum of an active phase and subsequent silent phase.

Processing and quantification of confocal images

To create high resolution, full-brain composite images, confocal stacks were digitally joined together using the Fiji (ImageJ) Pairwise Stitching[52] plug-in.

Quantification of presynaptic sites. Preparation of confocal images for analysis was performed in Fiji (ImageJ), in which individual colour channels were merged into a single TIFF file. Analysis was performed on vaa3d[53] by an analyser blinded to genotype. Puncta associated with labelled cell processes were manually counted and sorted by cell morphological location (for example, medulla layer). Manual counts for different cell types were cross-referenced with an automated feature detection algorithm to confirm count fidelity.

Counting Trpγ+ nuclei. Three-dimensional binary masks of the half-brain and one optic lobe were manually generated for each confocal stack using Fiji (ImageJ). Labelled nuclei were segmented from confocal stacks using custom scripts written in MATLAB and were assigned to different regions of the brain using the masks; a function critical to this task was sourced from the MathWorks File Exchange repository (T. Jerman (2021). Jerman Enhancement Filter (https://github.com/timjerman/JermanEnhancementFilter), GitHub.). The same segmentation approach was used to analyse the co-localization of glia and Trpγ+ nuclei (Extended Data Fig. 4c).

Statistical analysis

Statistical analysis was performed using RStudio. We used either unpaired, two-tailed Welch's t-test following the Shapiro–Wilk test for normality, or Tukey's post hoc test following ANOVA to assess statistical significance of differences between groups. Bonferroni corrections were applied to multiple comparisons where appropriate. Population averages are given as mean ± s.d. All measurements were taken from distinct samples.

Reporting summary

Further information on research design is available in the Nature Research Reporting Summary linked to this paper.

Data availability

The authors declare that all data supporting the findings of this study are available within the paper and its supplementary information files.

42. Bainbridge, S. P. & Bownes, M. Staging the metamorphosis of *Drosophila melanogaster*. *J. Embryol. Exp. Morphol.* **66**, 57–80 (1981).
43. Brand, A. H. & Perrimon, N. Targeted gene expression as a means of altering cell fates and generating dominant phenotypes. *Development* **118**, 401–415 (1993).
44. Lai, S. L. & Lee, T. Genetic mosaic with dual binary transcriptional systems in *Drosophila*. *Nat. Neurosci.* **9**, 703–709 (2006).
45. Piper, M. D. & Partridge, L. Protocols to study aging in *Drosophila*. *Methods Mol. Biol.* **1478**, 291–302 (2016).
46. Schindelin, J. et al. Fiji: an open-source platform for biological-image analysis. *Nat. Methods* **9**, 676–682 (2012).
47. Daniels, R. W. et al. Increased expression of the *Drosophila* vesicular glutamate transporter leads to excess glutamate release and a compensatory decrease in quantal content. *J. Neurosci.* **24**, 10466–10474 (2004).
48. Fei, H. et al. Mutation of the *Drosophila* vesicular GABA transporter disrupts visual figure detection. *J. Exp. Biol.* **213**, 1717–1730 (2010).
49. Park, D., Veenstra, J. A., Park, J. H. & Taghert, P. H. Mapping peptidergic cells in *Drosophila*: where DIMM fits in. *PLoS ONE* **3**, e1896 (2008).
50. Cabrero, P. et al. The *Dh* gene of *Drosophila melanogaster* encodes a diuretic peptide that acts through cyclic AMP. *J. Exp. Biol.* **205**, 3799–3807 (2002).
51. Terhzaz, S., Rosay, P., Goodwin, S. F. & Veenstra, J. A. The neuropeptide SIFamide modulates sexual behavior in *Drosophila*. *Biochem. Biophys. Res. Commun.* **352**, 305–310 (2007).
52. Preibisch, S., Saalfeld, S. & Tomancak, P. Globally optimal stitching of tiled 3D microscopic image acquisitions. *Bioinformatics* **25**, 1463–1465 (2009).
53. Peng, H., Ruan, Z., Long, F., Simpson, J. H. & Myers, E. W. V3D enables real-time 3D visualization and quantitative analysis of large-scale biological image data sets. *Nat. Biotechnol.* **28**, 348–353 (2010).

Acknowledgements We thank S. L. Zipursky for discussions, support and feedback on the manuscript; C. Montell for sharing fly lines and other reagents; T. R. Clandinin for support in generating the SPARC3-Out-GAL80 flies; J. M. Donlea, V. Hartenstein, D. E. Krantz and Y. Lin for sharing antibodies; J. A. Veenstra for sharing neuropeptide antibodies; D. Hattori for the Kir2.1 flies; A. Nern and G. M. Rubin for the 29C07-FLP flies; the Banerjee Laboratory at UCLA for the UAS-rpr,-hid flies; O. Kanca and H. J. Bellen for the *Trpγ*$^{DropIn\text{-}TG4}$ flies; S. Yamamoto and T. Takano-Shimizu for the UAS-TRPC4 and TRPC5 flies; and members of the Zipursky laboratory for feedback and discussion. B.T.B. is supported by NIH grants F30EY029952 and T32GM008042; OA is supported by NIH grant R01NS123376.

Author contributions B.T.B.: conceptualization, methodology, analysis, investigation and writing. N.T.P.: methodology, investigation (confocal microscopy) and writing (review and editing). J.I.-B.: methodology (SPARC), investigation and writing (review and editing). J.R.: methodology (assistance with TARGET system experiments, lifespan and eclosion analysis) and writing (review and editing). H.R.: investigation (dissections and assistance with image analysis) and writing (review and editing). O.A.: conceptualization, methodology, analysis, investigation, writing, project administration and funding acquisition.

Competing interests The authors declare no competing interests.

Additional information

Supplementary information The online version contains supplementary material available at https://doi.org/10.1038/s41586-022-04406-9.

Correspondence and requests for materials should be addressed to Orkun Akin.

Peer review information *Nature* thanks Gerald Rubin and the other, anonymous reviewers for their contribution to the peer review of this work.

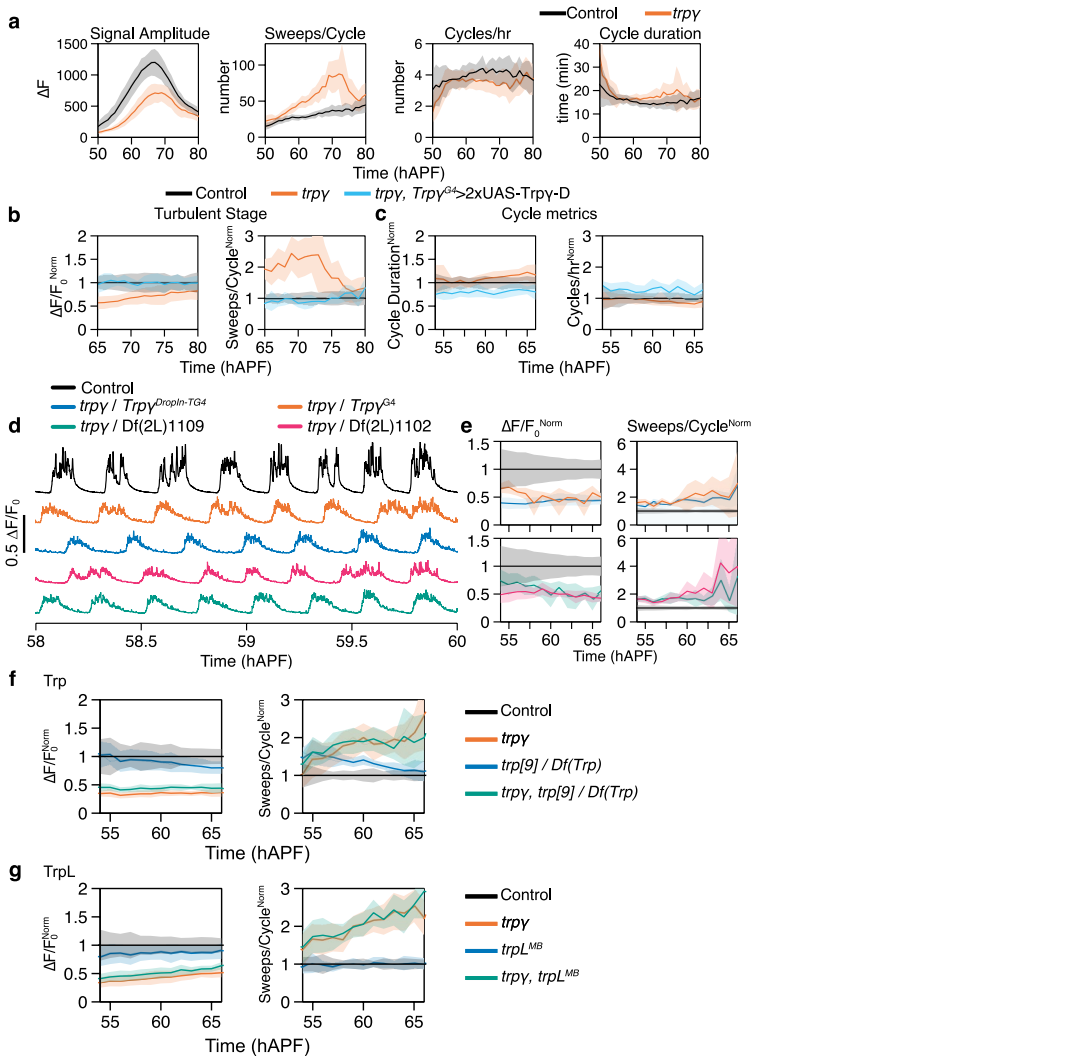

Extended Data Fig. 1 | *Trpγ* is necessary for PSINA. a. Raw values binned by hour for active phase signal amplitude, sweeps/cycle, cycles/hour, and cycle duration for control (black, n=19) and *trpγ* null (orange, n=31) pupae. Shaded areas, SD. **b**. Active phase average amplitude (left) and sweeps/cycle (right) binned by hour and normalized to control activity during the turbulent stage, between 65 and 80 hAPF, for control (black, n=19), *trpγ* null (orange, n=31), and *trpγ* null with Trpγ-D expressed in Trpγ+ cells (cyan, n=4) pupae. Shaded areas, SD. **c**. Cycle duration (left) and cycles/hour (right) binned by hour and normalized to control activity between 55 and 65 hAPF. Shaded areas, SD. Genotypes color-matched to B. **d**. Representative traces of activity in control (black, n=19), *trpγ*/*Trpγ*^{G4} (orange, n=5), *trpγ*/*Trpγ*$^{DropIn\text{-}TG4}$ (gray, n=5), *trpγ*/Df(2L)1102 (magenta, n=7), and *trpγ*/Df(2L)1109 pupae (green, n=7). **e**. Average amplitude (left) and sweeps/cycle (right) binned by hour and normalized to control activity between 55 and 65 hAPF. Shaded areas, SD. Genotypes color-matched to D. **f**. Active phase average amplitude (left) and sweeps/cycle (right) binned by hour and normalized to control activity during the periodic stage, between 55 and 65 hAPF, for control (black, n=10), *trpγ* null (orange, n=9), *trp* null (blue, n=10), and *trp* null + *trpγ* null (green, n=10). Shaded areas, SD. **g**. Active phase average amplitude (left) and sweeps/cycle (right) binned by hour and normalized to control activity during the periodic stage, between 55 and 65 hAPF, for control (black, n=10), *trpγ* null (orange, n=10), *trpL* null (blue, n=10), and *trpL* null+ *trpγ* null (green, n=10). Shaded areas, SD.

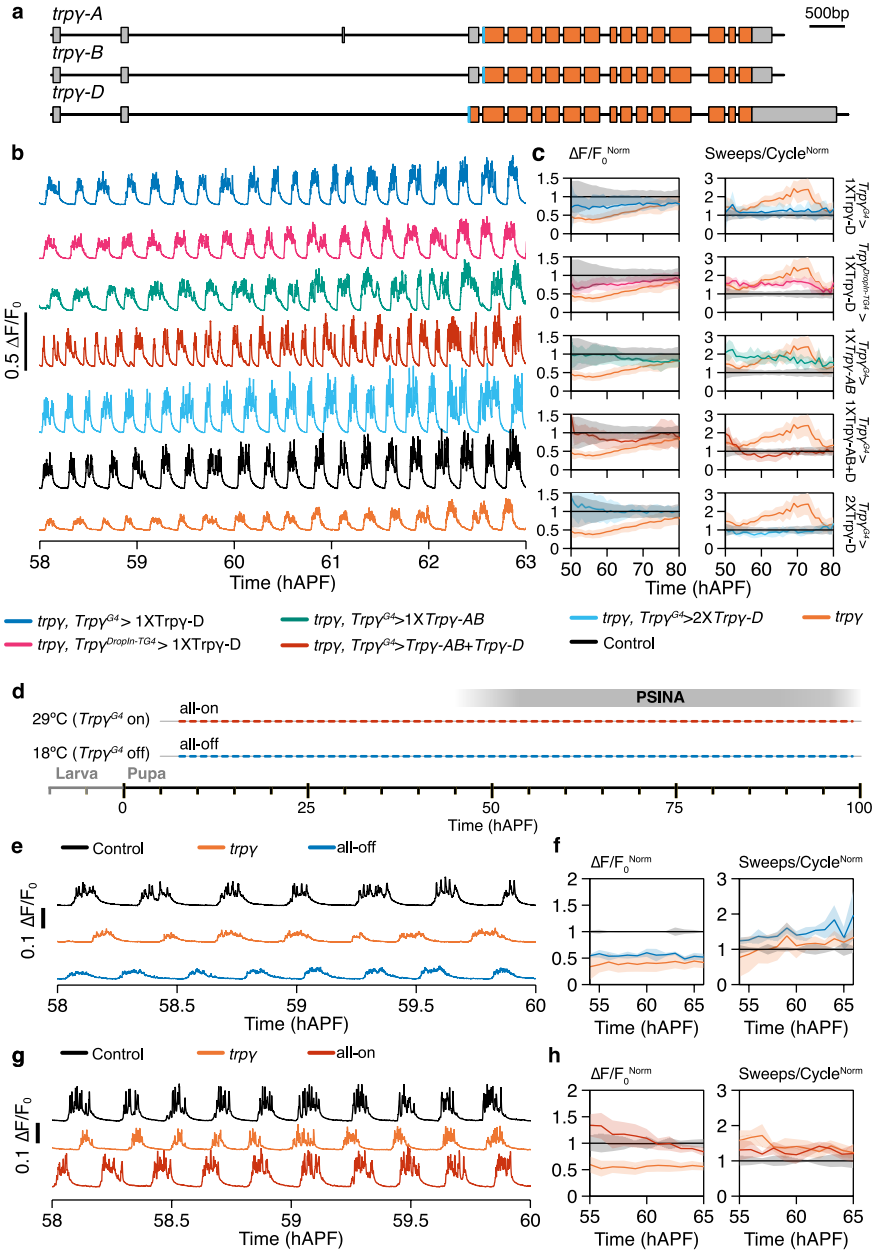

Extended Data Fig. 2 | PSINA rescue in *trpγ* null background. a. Schematic of *Trpγ* locus indicating locations of exons (orange rectangles), untranslated regions (gray rectangles), and introns (black lines between exons or untranslated regions) for each isoform. Scale bar, 500 bp. **b**. Representative traces of activity in: Trpγ-D expression with $Trpγ^{G4}$ (blue, n=8), Trpγ-D expression with $Trpγ^{DropIn\text{-}TG4}$ (magenta, n=7), Trpγ-AB expression with $Trpγ^{G4}$ (green, n=9), Trpγ-AB and Trpγ-D expression with $Trpγ^{G4}$ (red, n=10), double Trpγ-D expression with $Trpγ^{G4}$ (cyan, n=4), control (black, n=19), and *trpγ* mutant (orange, n=31) pupae. **c**. Active phase average amplitude (left) and sweeps/cycle (right) binned by hour and normalized to control activity between 55 and 65 hAPF. All plots contain data for control (black) and *trpγ* (orange). Shaded areas, SD. Genotypes color-matched to B. **d**. Expression control of UAS-Trpγ-D with TARGET (i.e. GAL80ts). In the 'all-on' condition, flies are reared at 29°C. In the 'all-off' condition, flies are reared at 18°C. **e, g**. Representative traces of activity in control pupae (black, n=3), *trpγ* null pupae (orange, n=3), and (E) all-off pupae (blue, n=3) or (G) all-on pupae (red, n=3). **f, h**. Active phase average amplitude (left) and sweeps/cycle (right) binned by hour and normalized to control activity between 55 and 65 hAPF. Shaded areas, SD. Genotypes color-matched to E and G.

a Wildtype medulla synapse counts

Cell Type	Takemura et al., 2008	Takemura et al., 2013	Chen et al., 2014	This work
R8	35 ± 1 (n = 3)	50 (n = 1)	46 ± 5 (n = 30)	50 ± 6 (n = 46)
L4	22 ± 2 (n = 3)	26 (n = 1)	26 ± 4 (n = 30)	22 ± 3 (n = 44)

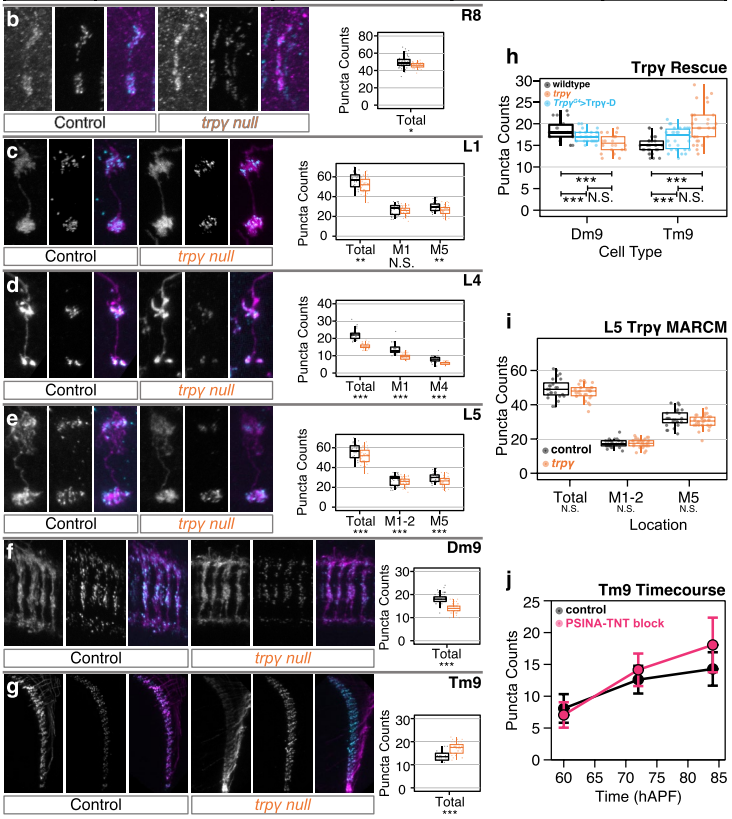

Extended Data Fig. 3 | Synapse formation in the visual system depends on PSINA. a. Table comparing control synapse counts in cells with sparse synaptic density across EM and light microscopy studies. Values are mean synapse count ± SD, with sample size in parentheses. **b**–**g**. *Left*: representative micrographs of R8 (B), L1 (C), L4 (D), L5 (E), Dm9 (F), and Tm9 (G) neurons in control (left set) and *trpγ* (right set) animals with cell membranes (myr::tdTOM, magenta in merged) and presynaptic sites (BRP-V5, cyan in merged) labeled. *Right*: Brp puncta counts by layer in heterozygous control (black, n=18-61 per cell type) and *trpγ* (orange, n=26-65 per cell type) animals. Points indicate individual cells. Box-and-whiskers mark 5th, 25th, 50th, 75th, and 95th percentiles. *, p<0.05; **, p<0.01; ***, p<0.001 by Welch's t-test following Shapiro-Wilk test. **h**. Brp puncta counts in *Trpγ* heterozygotes (black, n=18 for Dm9, n=30 for Tm9), *trpγ* nulls (orange, n=24 for Dm9, n=30 for Tm9), or *trpγ* nulls with Trpγ-D expressed in Trpγ+ cells (cyan, n=24 for Dm9, n=30 for Tm9). Boxplots as in B-G. *, p<0.05; **, p<0.01; ***, p<0.001 by Tukey's post-hoc test following ANOVA for multiple groups. **i**. Brp puncta counts in control (black, n = 24) or *trpγ* null (orange, n = 30) L5 clones generated by MARCM. Boxplots as in B-G. *, p<0.05; **, p<0.01; ***, p<0.001 by Welch's t-test following Shapiro-Wilk test. **j**. Average Brp puncta through development in control (black, n=64-88 per timepoint) or animals with PSINA blocked with pan-neuronally expressed TNT (magenta, n=35-68 per timepoint). Presynaptic sites assessed at 60, 72, and 84 hAPF. Error bars, SD.

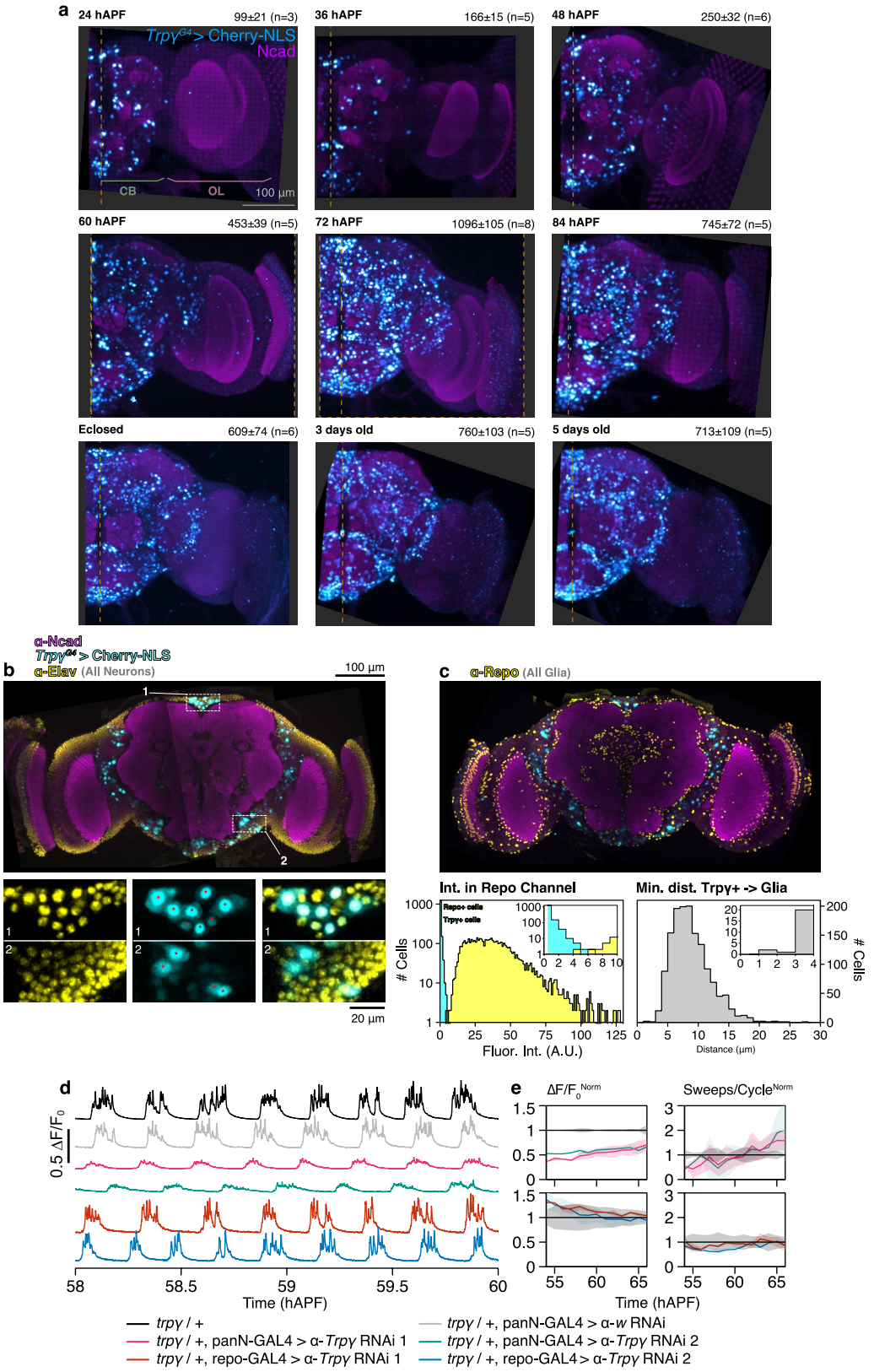

Extended Data Fig. 4 | See next page for caption.

Extended Data Fig. 4 | *Trpγ*^{G4} drives expression in a dynamic neuronal population during development. a. MIPs of half-brain confocal stacks from different times during pupal development and early adult life. Nuclei of mCherry-NLS expressing Trpγ+ neurons shown (cyan); reference marker is Ncad (magenta). Average, SD, and number of samples for each time point are printed top-right of panels; these values are plotted in Fig. 4a. Dashed yellow lines mark the median plane. CB, central brain. OL, optic lobe. Scale bar, 100µm. **b**. *Top:* 13µm-thick MIP of a 72 hAPF brain stained for neuronal nuclei (anti-Elav, yellow), Trpγ+ nuclei (mCherry-NLS, cyan), and a reference marker (Ncad, magenta). Image derived from three stitched confocal stacks. Scale bar, 100µm. *Bottom:* Expanded views of two regions-of-interest (ROIs) boxed in top panel. Columns are neuronal, Trpγ+, and merged channels, left to right. All Trpγ+ nuclei fully captured in the MIP (red asterisks) co-localize with the neuronal stain. Scale bar, 20µm. **c**. *Top:* 13µm-thick MIP of a 72 hAPF brain stained for glial nuclei (anti-Repo, yellow), Trpγ+ nuclei (mCherry-NLS, cyan), and a reference marker (Ncad, magenta). Image derived from three stitched confocal stacks. Scale bar, 100µm. *Bottom-left:* Histogram of average voxel intensities of segmented Repo+ and Trpγ+ nuclei measured in the anti-Repo channel of the top image. n=5055 (Repo+), 1464 (Trpγ+); half-brain complements analyzed. Inset shows where 9/1464 Trpγ+ cell intensities overlap with the dimmest Repo+ glia. *Bottom-right:* Histogram of minimum pairwise distance between centroids of 1464 segmented Trpγ+ and Repo+ nuclei. Inset shows all pairs of Trpγ+ and Repo+ nuclei are at least 1µm apart. **d**. Representative traces of activity in control pupae (black), pan-neuronal control knockdown pupae (gray, n=2), pan-neuronal *Trpγ* knockdown (magenta, n=3; green, n =3), pan-glial *Trpγ* knockdown (red, n=2; blue, n=2) in heterozygous *Trpγ* background. **e**. Active phase average amplitude (left) and sweeps/cycle (right) binned by hour and normalized to control activity between 55 and 65 hAPF. Shaded areas, SD. Genotypes color-matched to D.

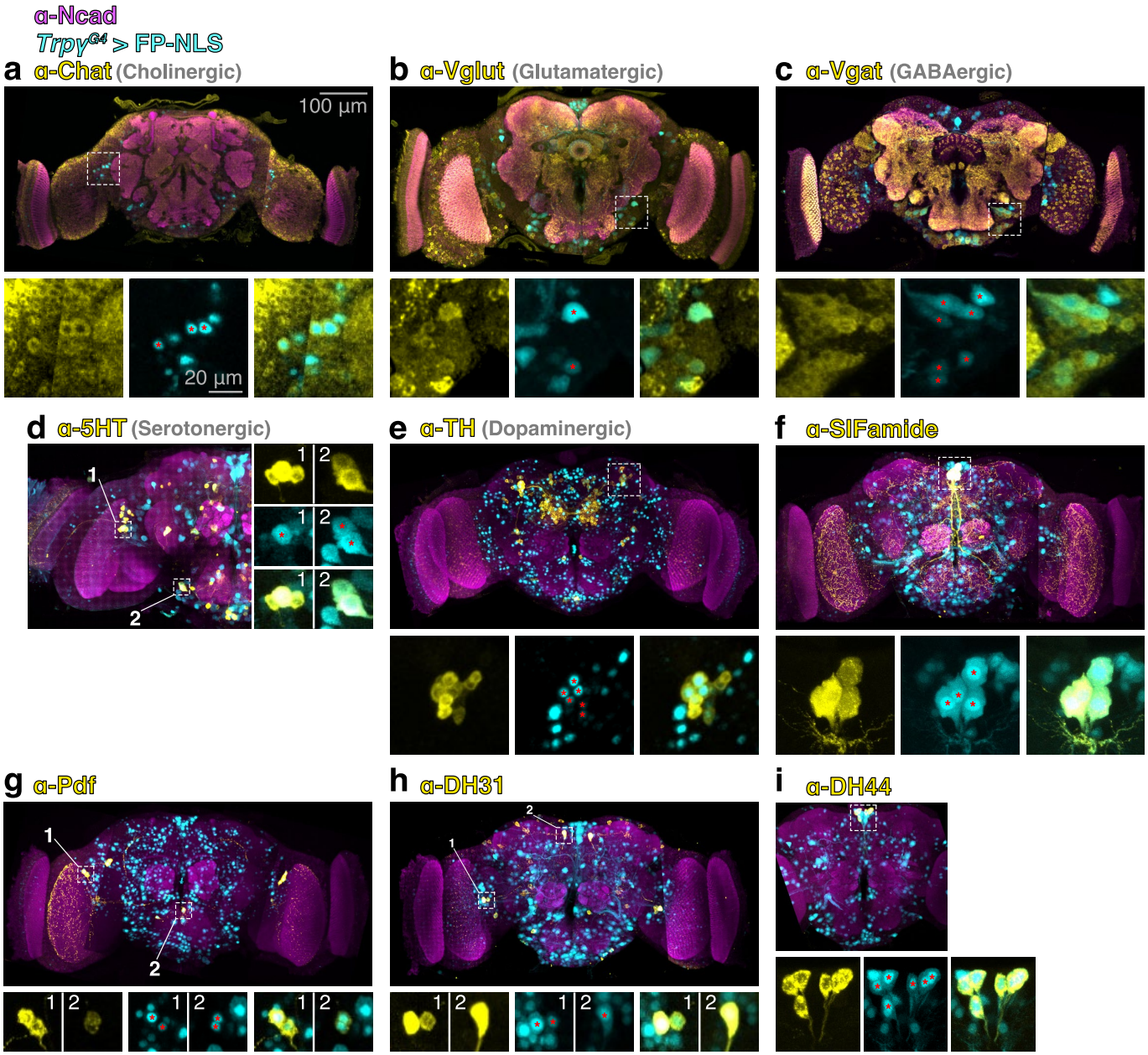

Extended Data Fig. 5 | Trpγ+ neurons are a diverse population. a–i. *Top:* 13µm-thick (A-C) or full (D-I) MIPs of 72 hAPF brains stained for neuronal class marker (yellow), Trpγ+ nuclei (mCherry-NLS or GFP-NLS, cyan), and a reference marker (Ncad, magenta). Images (A-C, E-H) derived from three stitched confocal stacks. Scale bar, 100µm. *Bottom:* Expanded view(s) of ROI(s) boxed in top panel. Columns (D, rows) are class marker, Trpγ+, and merged channels, left to right (D, top to bottom). Marked Trpγ+ nuclei (red asterisks) co-localize with the neuronal class marker. ROI 2 in (G) shows transient PDF-TRI cells (*38*). Scale bar, 20µm.

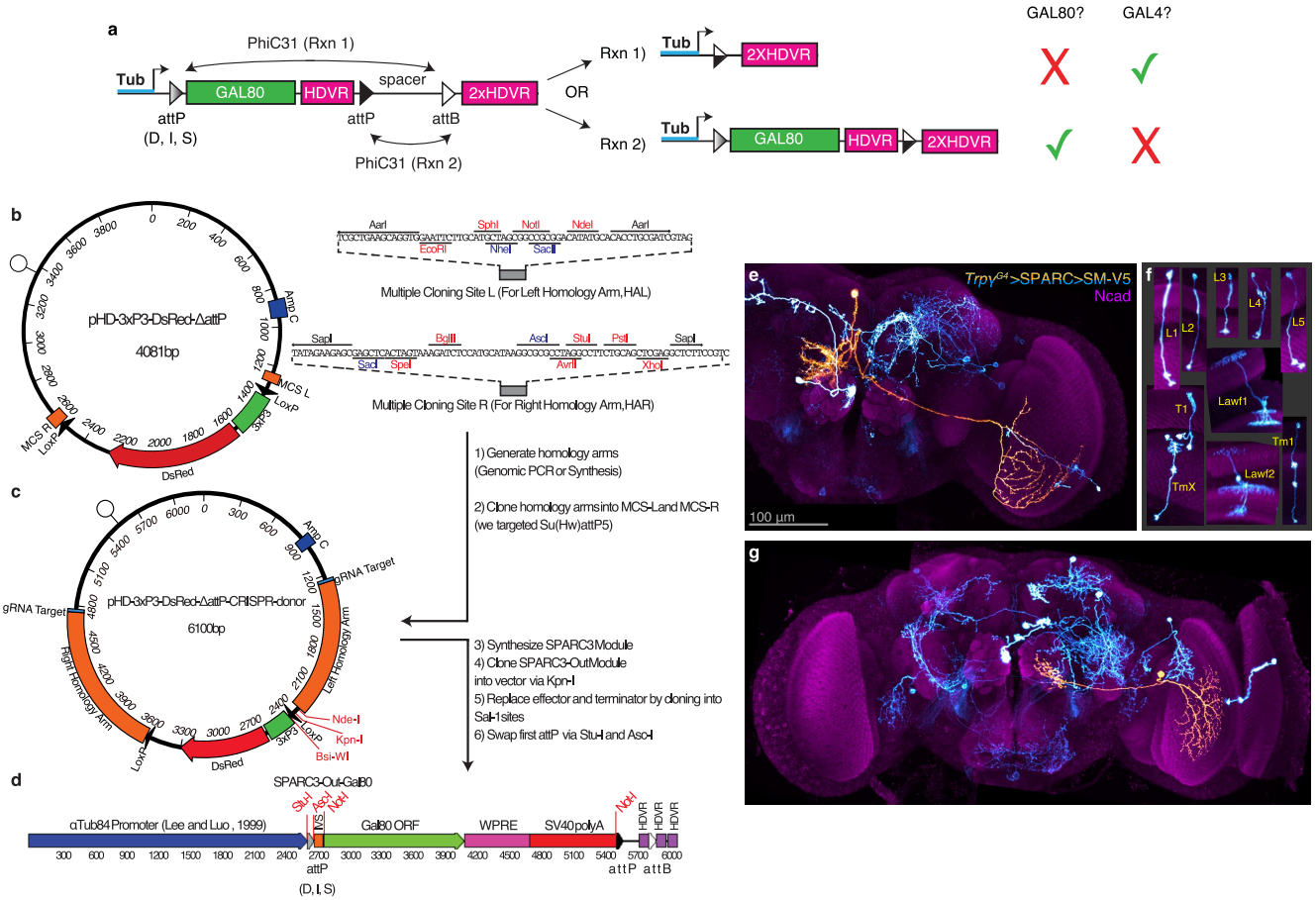

Extended Data Fig. 6 | SPARC3-Out-GAL80 reveals morphologies of individual Trpγ+ neurons. a. Schematic of the SPARC3-Out-GAL80 cassette. PhiC31 recombines one of two competing *attP* target sequences with one *attB* target sequence. Rxn 1 leads to loss of the GAL80 ORF, disinhibiting GAL4-driven effector expression. Rxn 2 preserves Tubulin promoter driven GAL80 expression, maintaining GAL4 inhibition. Three progressively truncated variants for the first *attP* sequence were designed (*25*) to bias the recombination in favor of Rxn 2, resulting in frequent (Dense), sporadic (Intermediate), or rare (Sparse) loss of GAL80 and disinhibition of GAL4>UAS expression. **b**. Map of pHD-3xP3-DsRed-Δ*attP* (a CRISPR-HDR-donor precursor) showing multiple cloning sites for homology arm insertion (right). **c**. Map of pHD-3xP3-DsRed-Δ*attP*-CRISPR-donor (example includes homology arms targeting the *Su(Hw)AttP5* region of the *Drosophila* genome). **d**. Assembled SPARC3-Out-GAL80 cassette; see Materials and Methods for details. MCS, multiple cloning site. gRNA, guide RNA. HDVR, hepatitis delta virus ribozyme sequence. **e, g**. Single Trpγ+ neuron (orange, manually segmented) in the context of others (cyan) labeled using SPARC. Neurons expressing myr::SM-V5. Reference marker (magenta), Ncad. Image MIP of stitched confocal stacks of 72 hAPF brain. Scale bar, 100µm. **f**. Trpγ+ visual processing neurons identified in 72 hAPF brains using SPARC. We observed a given neuron up to three times in 30 sparsely labeled brains.

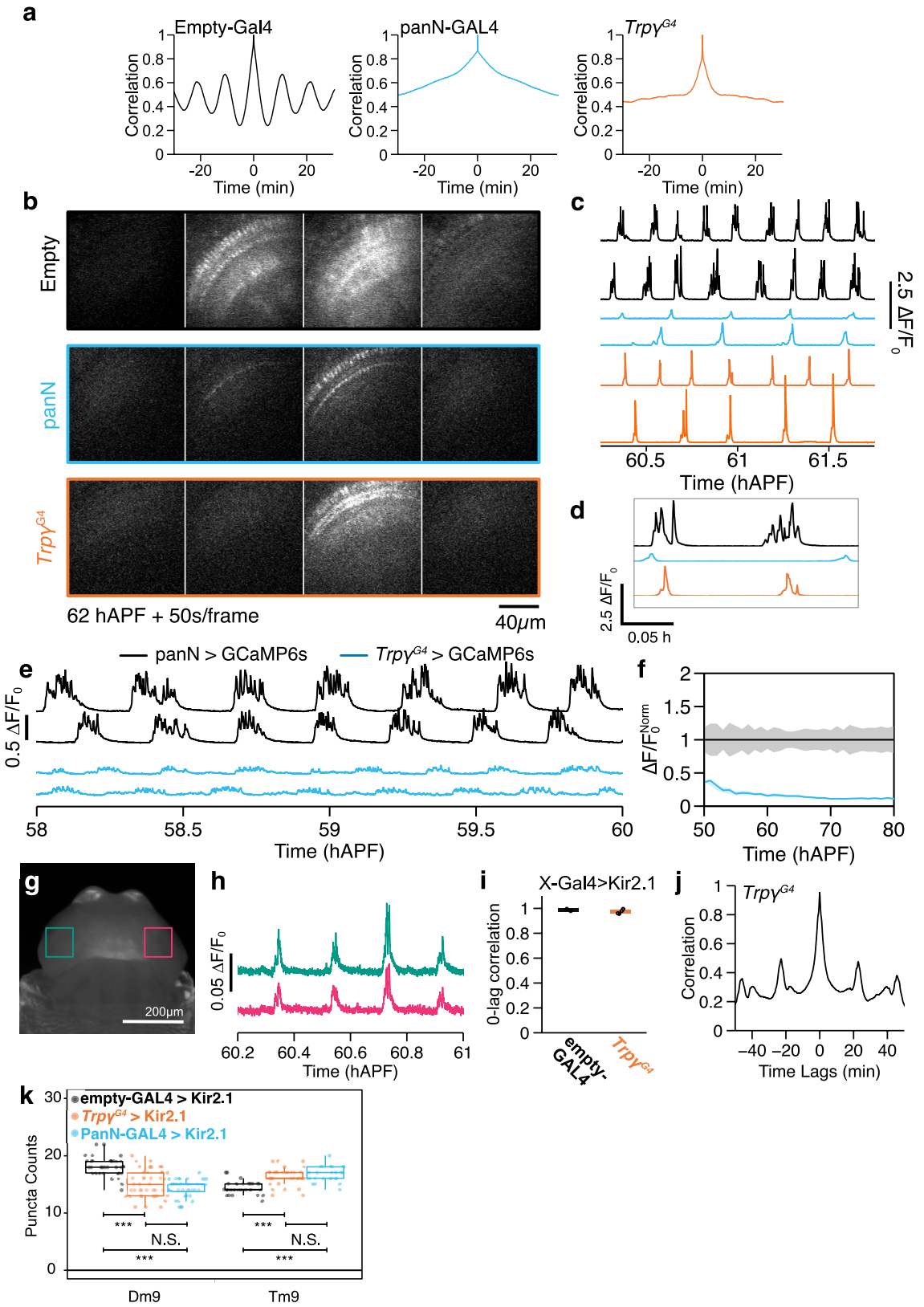

Extended Data Fig. 7 | See next page for caption.

Extended Data Fig. 7 | Additional characterization of Trpγ+ neuron activity. a. Representative autocorrelograms from pan-neuronal GCaMP6s in control (empty-GAL4, black), panN-GAL4>Kir2.1 (blue), and $Trp\gamma^{G4}$>Kir2.1 (orange) pupae. **b, c**. Representative micrographs (B) and traces (C) from 2PM imaging of pan-neuronal GCaMP6s in control (empty-GAL4, black), panN-GAL4>Kir2.1 (blue), and $Trp\gamma^{G4}$>Kir2.1 (orange) pupae. Scale bar, 40µm. **d**. *Inset*: expanded view showing fewer sweeps in panN-GAL4 and $Trp\gamma^{G4}$ conditions. **e**. Representative traces for Trpγ+ neurons expressing GCaMP6s (cyan, n=10) and pan-neuronal expression of GCaMP6s (black, n=10) by wide-field imaging with a ROI encompassing the head. **f**. Active phase average amplitude for Trpγ+ neurons expressing GCaMP6s (cyan) binned by hour and normalized to pan-neuronal expression of GCaMP6s (black). Shaded areas, SD. **g, h**. AIP of pupae expressing pan-neuronal GCaMP6s (g). ROIs indicate regions used to calculate traces (h) from optic lobes. Scale bar, 200µm. **i**. 0-lag correlation between traces in each optic lobe in control (empty-GAL4, black, n=4), and $Trp\gamma^{G4}$>Kir2.1 (orange, n=4) pupae. Round markers are values from individual time series, bars are averages for each genotype. **j**. Correlogram between traces in each optic lobe in $Trp\gamma^{G4}$>Kir2.1 pupa. **k**. Cell-type-specific Brp puncta counts in control (empty-GAL4>Kir2.1 pupae, black, n=35 per cell type), PanN-GAL4>Kir2.1 pupae (cyan, n=40 for Dm9, n=25 for Tm9) and in $Trp\gamma^{G4}$>Kir2.1 pupae (orange, n=40 cells for Dm9, n=35 cells for Tm9).

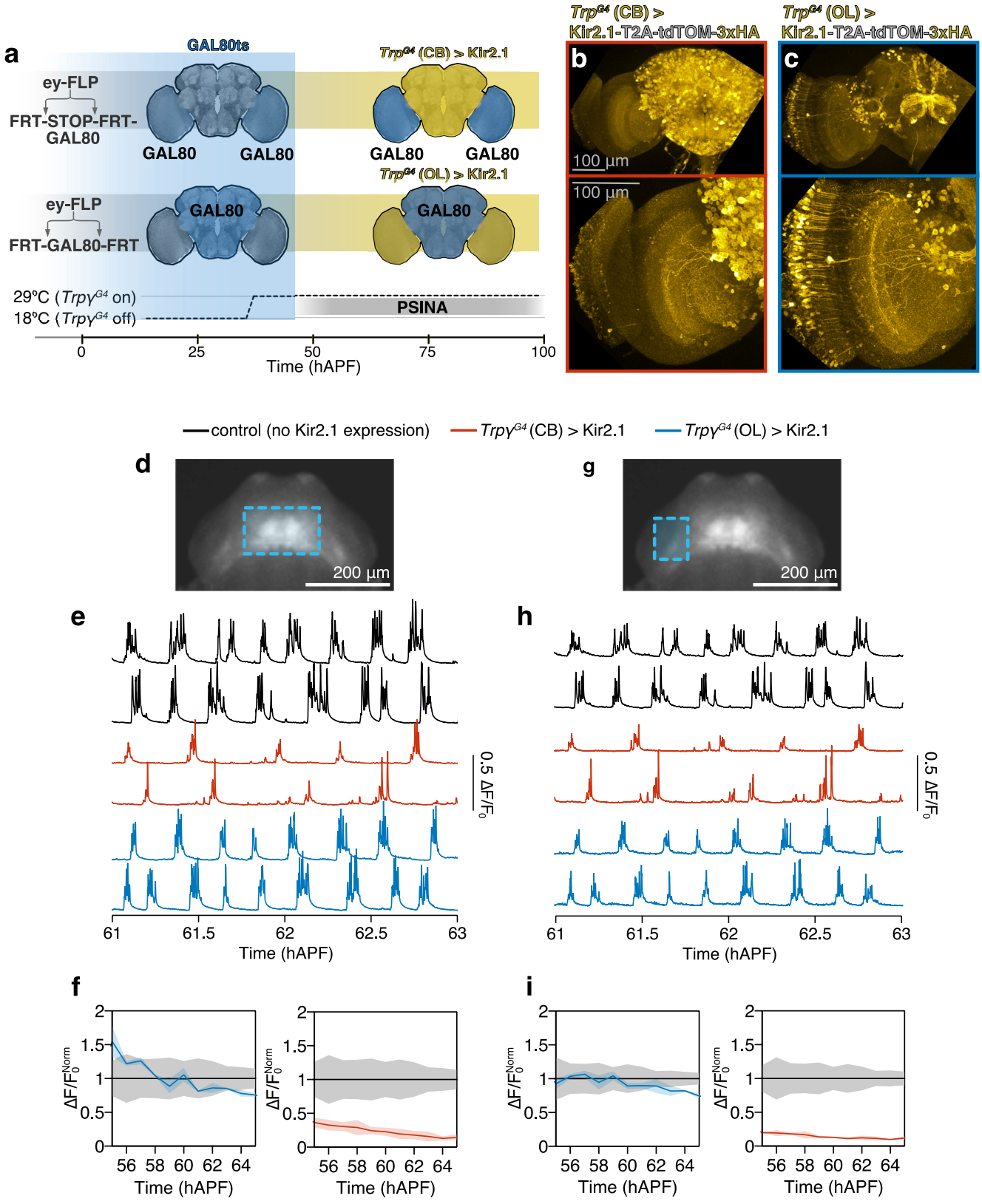

Extended Data Fig. 8 | See next page for caption.

Extended Data Fig. 8 | Silencing Trpγ+ neurons in the central brain, but not the optic lobes, attenuates PSINA. a. Schematic of spatially-targeted Kir2.1 expression. Both experimental genotypes carry two variants of tubP-GAL80: GAL80ts and one of two FLP-responsive conditional alleles. In the optic lobes, ey-FLP either turns on GAL80 expression by removing the interruption cassette ('-STOP-', top) or turns it off by locally excising the FRT-flanked ORF (bottom). Animals are reared at 18°C and shifted 29°C at 40 hAPF to unmask these differential GAL80 expression domains (blue) just prior to PSINA onset; GAL4-driven Kir2.1 expression is disinhibited in the complementary domains (yellow). CB, central brain. OL, optic lobe. **b**, **c**. MIPs of half-brains (top) or optic lobes (bottom) at 60 hAPF in which $Trp\gamma^{G4}$ is driving Kir2.1 expression in the CB (B) or the OL (C). The OL condition also includes expression in the antennal lobes and a small number of CB neurons. Kir2.1 expression domain detected by staining against 3xHA tagged co-cistronic tdTOM. Scale bar, 100µm. **d, g**. AIP of ~60 hAPF pupa expressing GCaMP6s pan-neuronally. CB (D) and OL (G) ROIs used for measuring PSINA outlined (cyan). Scale bar, 200µm. **e, h**. PSINA traces from CB (E) and OL (H) for control (no Kir2.1, black, n=5), $Trp\gamma^{G4}$(CB)>Kir2.1 (red, n=3), and $Trp\gamma^{G4}$(OL)>Kir2.1 (blue, n=3) genotypes. **f, i**. Average amplitude measured in CB (F) and OL (G) normalized to corresponding control activity. Shaded areas, SD. Genotypes color-matched to E.

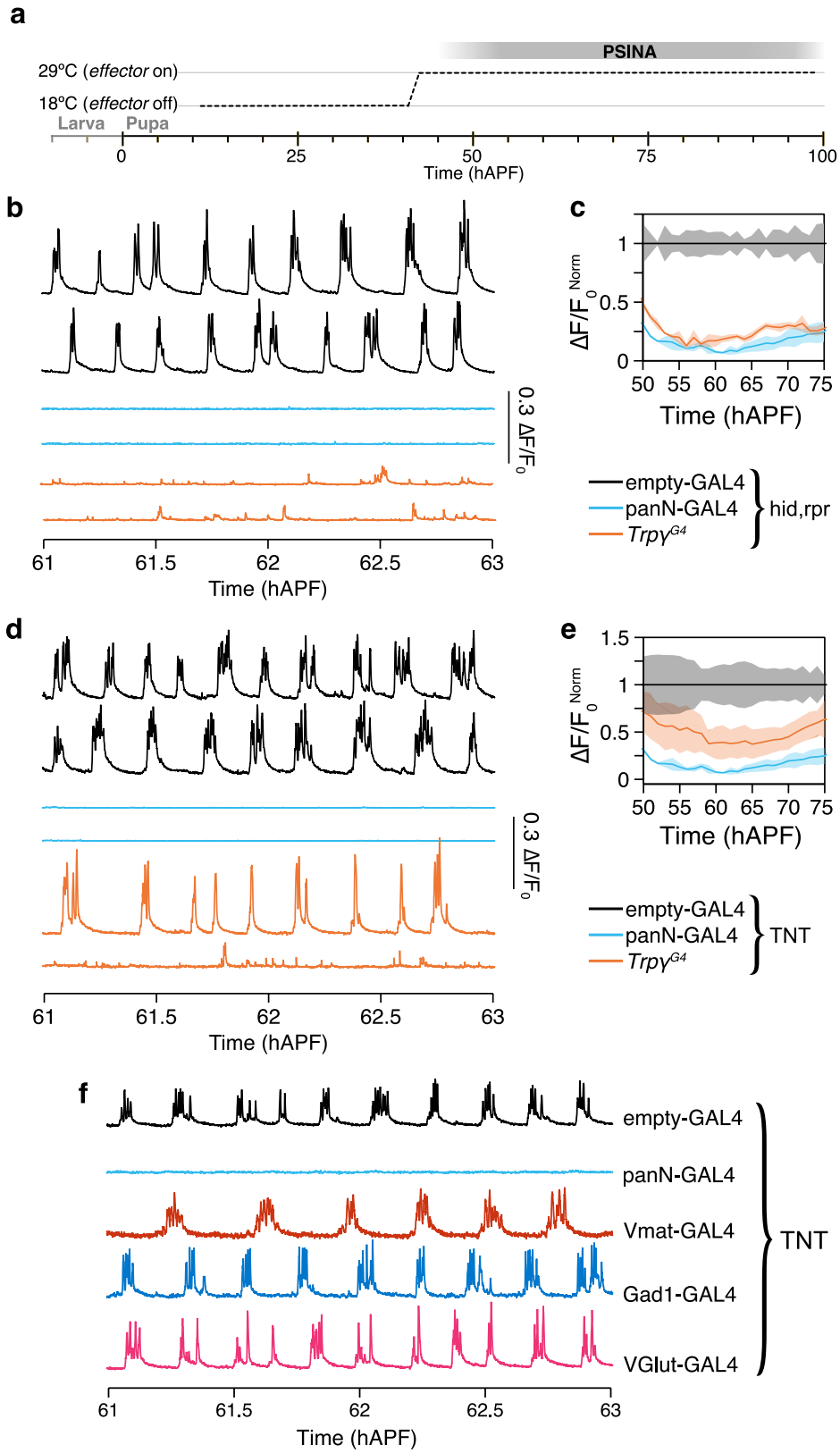

Extended Data Fig. 9 | Trpγ+ neurons are necessary for PSINA. a. Temporal expression control with TARGET; animals shifted from 18°C to 29°C at 40 hAPF. **b**. PSINA traces from pan-neuronal GCaMP6s in control (empty-GAL4, black, n=3), panN-GAL4>hid, rpr (blue, n=3), and *Trpγ*^{G4}>hid, rpr (orange, n=3) pupae. **c**. Average amplitude normalized to control activity between 55 and 75 hAPF. Shaded areas, SD. Genotypes color-matched to B. **d**. PSINA traces from pan-neuronal GCaMP6s in control (empty-GAL4, black, n=7), panN-GAL4>TNT (blue, n=7), and *Trpγ*^{G4}>TNT (orange, n=8) pupae. **e**. Average amplitude normalized to control activity between 55 and 75 hAPF. Shaded areas, SD. Genotypes color-matched to D. **f**. Representative traces of pupae expressing pan-neuronal GCaMP6s, with TNT expressed in expression domains of the indicated neuronal class. n=4 tested for each genotype.

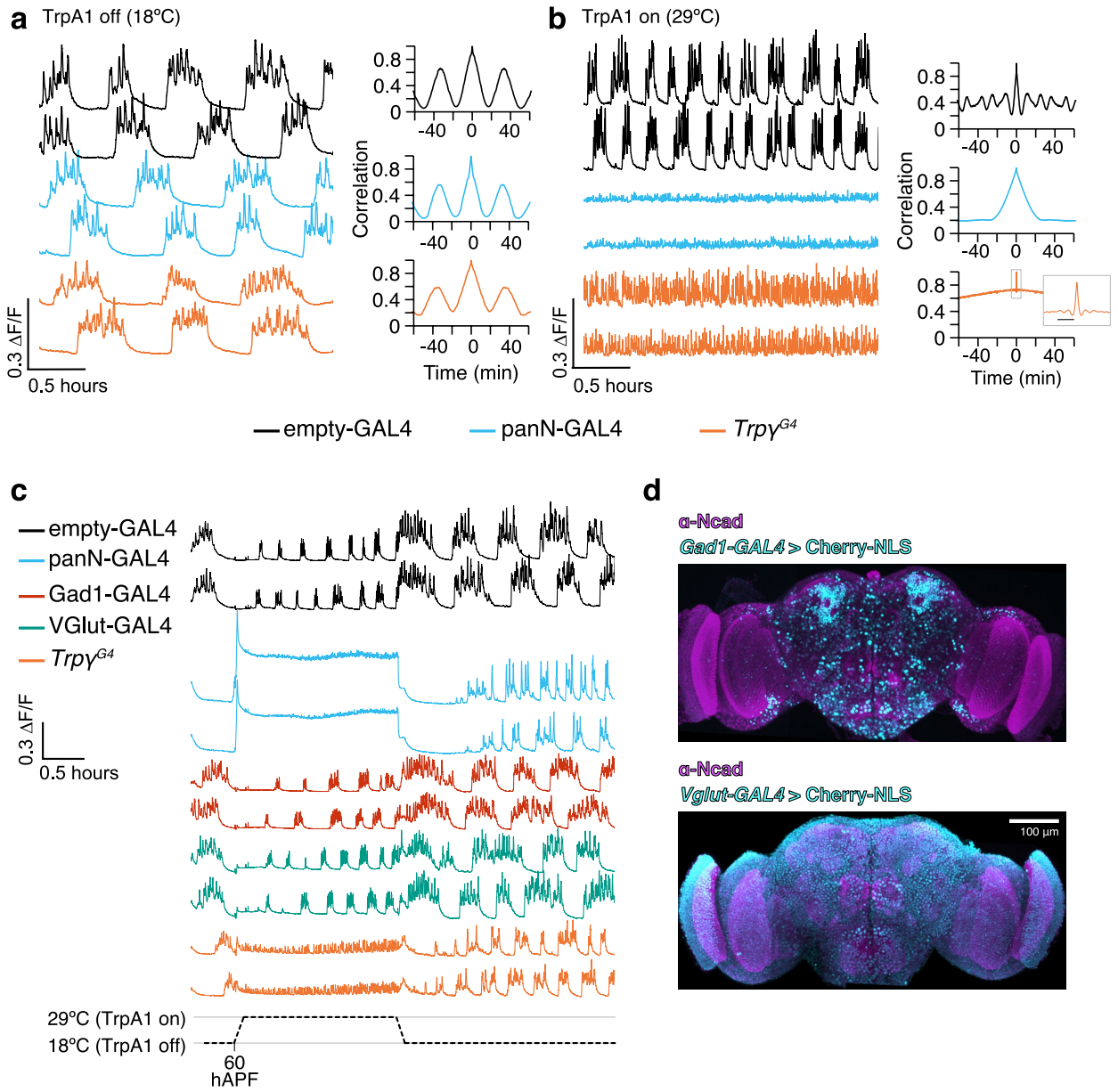

Extended Data Fig. 10 | Activation of Trpγ+ neurons increases brain-wide activity frequency. a, **b**. *Left*: PSINA traces from pan-neuronal GCaMP6s in control (empty-GAL4, black, n=3), panN-GAL4>TrpA1 (blue, n=3), and *Trpγ*^{G4}>TrpA1 (orange, n=3) pupae at 18°C (A) or 29°C (B). *Right*: representative auto-correlograms calculated from the first trace shown for each genotype. *Inset (B)*: expanded view of boxed region. Scale bar, 2min. **c**. Activity from pan-neuronal GCaMP6s in control (empty-GAL4, black, n=6), panN-GAL4>TRpA1 (blue, n=6), VGlut-GAL4>TrpA1 (red, n=6), Gad1-GAL4 (green, n=5), *Trpγ*^{G4}>TrpA1 (orange, n=6) pupae at 60 hAPF. Pupae reared at 18°C and shifted to 29°C. **d**. MIPs of 60 hAPF brains stained for a nuclear marker (Cherry-NLS, cyan) driven by *Gad1-* or *Vglut-GAL4*, and a reference marker (Ncad, magenta). Images derived from three stitched confocal stacks. Scale bar, 100µm. **e**. Conceptual circuit organizations for coordinating and propagating PSINA. Metronomes indicate CPGs. Colored arrows indicate Trpγ+ and other relay neurons.

nature research

Corresponding author(s): Orkun Akin

Last updated by author(s): Feb 26, 2021

Reporting Summary

Nature Research wishes to improve the reproducibility of the work that we publish. This form provides structure for consistency and transparency in reporting. For further information on Nature Research policies, see our Editorial Policies and the Editorial Policy Checklist.

Statistics

For all statistical analyses, confirm that the following items are present in the figure legend, table legend, main text, or Methods section.

n/a	Confirmed	
☐	☒	The exact sample size (*n*) for each experimental group/condition, given as a discrete number and unit of measurement
☐	☒	A statement on whether measurements were taken from distinct samples or whether the same sample was measured repeatedly
☐	☒	The statistical test(s) used AND whether they are one- or two-sided *Only common tests should be described solely by name; describe more complex techniques in the Methods section.*
☒	☐	A description of all covariates tested
☐	☒	A description of any assumptions or corrections, such as tests of normality and adjustment for multiple comparisons
☐	☒	A full description of the statistical parameters including central tendency (e.g. means) or other basic estimates (e.g. regression coefficient) AND variation (e.g. standard deviation) or associated estimates of uncertainty (e.g. confidence intervals)
☐	☒	For null hypothesis testing, the test statistic (e.g. *F*, *t*, *r*) with confidence intervals, effect sizes, degrees of freedom and *P* value noted *Give P values as exact values whenever suitable.*
☒	☐	For Bayesian analysis, information on the choice of priors and Markov chain Monte Carlo settings
☒	☐	For hierarchical and complex designs, identification of the appropriate level for tests and full reporting of outcomes
☒	☐	Estimates of effect sizes (e.g. Cohen's *d*, Pearson's *r*), indicating how they were calculated

Our web collection on statistics for biologists contains articles on many of the points above.

Software and code

Policy information about availability of computer code

Data collection	SlideBook (Intelligent Imaging, Inc.) and Zen (Zeiss) software were used to acquire images.
Data analysis	Fiji, Matlab (Mathworks, Inc.)

For manuscripts utilizing custom algorithms or software that are central to the research but not yet described in published literature, software must be made available to editors and reviewers. We strongly encourage code deposition in a community repository (e.g. GitHub). See the Nature Research guidelines for submitting code & software for further information.

Data

Policy information about availability of data

All manuscripts must include a data availability statement. This statement should provide the following information, where applicable:

- Accession codes, unique identifiers, or web links for publicly available datasets
- A list of figures that have associated raw data
- A description of any restrictions on data availability

All raw or processed data will be made available upon request.

Field-specific reporting

Please select the one below that is the best fit for your research. If you are not sure, read the appropriate sections before making your selection.

☒ Life sciences ☐ Behavioural & social sciences ☐ Ecological, evolutionary & environmental sciences

For a reference copy of the document with all sections, see nature.com/documents/nr-reporting-summary-flat.pdf

Life sciences study design

All studies must disclose on these points even when the disclosure is negative.

Sample size	For calcium imaging experiments and immunohistochemistry experiments, n=3 was chosen as the minimum replicate number, and sample size was determined by the number of animals that were expressing the calcium indicator and were appropriately staged for developmental imaging. For counting presynaptic sites, n = 20 was chosen as the minimum replicate number, and sample size was determined by the number of cells that had positive signal in both imaging channels and could be resolved from neighboring cells. These sample sizes were determined to be sufficient due to low observed variability between samples.
Data exclusions	Data were not excluded from analysis.
Replication	All experiments were performed with technical replicates, and all replications were successful.
Randomization	Organisms within a given genotype were selected randomly from bottles and staged for developmental time. Organisms with appropriate developmental age were selected for subsequent experiments.
Blinding	For counting presynaptic sites, the analyzer was blinded to genotype while counting puncta. For other histology or calcium imaging experiments, blinding was not possible. However, quantifications were performed using a computational pipeline equally applied to all conditions and replicates.

Reporting for specific materials, systems and methods

We require information from authors about some types of materials, experimental systems and methods used in many studies. Here, indicate whether each material, system or method listed is relevant to your study. If you are not sure if a list item applies to your research, read the appropriate section before selecting a response.

Materials & experimental systems

n/a	Involved in the study
☐	☒ Antibodies
☒	☐ Eukaryotic cell lines
☒	☐ Palaeontology and archaeology
☐	☒ Animals and other organisms
☒	☐ Human research participants
☒	☐ Clinical data
☒	☐ Dual use research of concern

Methods

n/a	Involved in the study
☒	☐ ChIP-seq
☒	☐ Flow cytometry
☒	☐ MRI-based neuroimaging

Antibodies

Antibodies used	Mouse monoclonal anti-V5 (Novus Biologicals #NBP2-52703-0.2mg, 1:150), rat monoclonal anti-FLAG (DYKDDDDK) (Novus Biologicals #NBP1-06712, 1:100), mouse monoclonal anti-c-MYC (Developmental Studies Hybridoma Bank (DSHB) #9E10-concentrate, 1:100), rabbit polyclonal anti-dsRed (Clontech #632496, 1:125), chicken anti-GFP (Abcam #ab13970, 1:1000), rabbit monoclonal anti-HA (Cell Signaling Technology #3724, 1:300), rat monoclonal anti-Ncad (DSHB #DN-Ex #8-c, 1:100), mouse monoclonal anti-Elav (DHSB #Elav-9F8A9, 1:100), mouse monoclonal anti-Repo (DHSB #8D12 anti-Repo, 1:100), mouse monoclonal anti-Chat (DHSB #ChAT4B1, 1:20), mouse monoclonal anti-Pdf (DHSB #PDF C7, 1:1000), rabbit polyclonal anti-DVGLUT (1:1000), rabbit polyclonal anti-DVGAT (1:200), mouse monoclonal anti-TH (Immunostar #22941, 1:200), rabbit polyclonal anti-5-HT (Immunostar #20080, 1:1000), rabbit polyclonal anti-DH31 (1:1000), rabbit polyclonal anti-DH44 (1:1000), rabbit polyclonal anti-SIFamide (1:1000). Secondary antibodies and dilutions used in this study were as follows: Alexa 488 donkey polyclonal anti-chicken (Jackson ImmunoResearch # 703-545-155, 1:400), Alexa 488 donkey polyclonal anti-mouse (Jackson ImmunoResearch #715-545-151, 1:400), Alexa 568 donkey polyclonal anti-rabbit (Invitrogen #A10042, 1:400), Alexa 647 donkey polyclonal anti-rat (Jackson ImmunoResearch #712-605-153, 1:400).
Validation	Antibodies against epitope tags, anti-NCad, anti-Elav, and anti-Repo have been previously validated in Drosophila (e.g. Chen et al., 2014). Primary antibodies against neuropeptides and neurotransmitters have been previously validated (see the following publications: R. W. Daniels et al., J Neurosci 2004, H. Fei et al., J Exp Biol 2010, D. Park, J. A. Veenstra, J. H. Park, P. H. Taghert, PLoS One 2008, P. Cabrero et al., J Exp Biol 2002, S. Terhzaz et al., Biochem Biophys Res Commun 2007.)

Animals and other organisms

Policy information about studies involving animals; ARRIVE guidelines recommended for reporting animal research

Laboratory animals	Drosophila melanogaster (female unless otherwise noted) were used for experiments. Genotypes for each experiment can be found in TableS1.
Wild animals	N/A.
Field-collected samples	N/A.
Ethics oversight	No ethical oversight committee was required for use of Drosophila samples.

Note that full information on the approval of the study protocol must also be provided in the manuscript.